Contents

Chapter 1

Introduction and literature review

1.1 Introduction

In the industrial processes thermal characteristics of fluids have a crucial function in heating and cooling applications. Thermal conductivity of a fluid is significant physical characteristic which decides its heat transit performance. Conventional heat transit fluids have intrinsically weaker thermal conductivity. In case of ultra-high cooling, thermal conductivity makes the fluid incapable. For effective traits of mixtures, researchers have attempted to develop the inherently weaker thermal conductivity of these ordinary heat transit fluids by using CEMT (classical effective medium theory) of Maxwell [1]. To get better heat transit performance, fine adjustment of these solid suspensions to millimeter and micrometer ranges have failed due to some drawbacks like particle sedimentation, poor thermal conductivity, particle clogging, and extravagant pressure drop.

All properties of a substance vary due to a critical scale of physical mechanism. Current nanotechnology present physical and chemical means to prepare nanometer sized particles on the molecular scales with improved thermo-physical properties as compared to their relevant bulk structures. It has been demonstrated by Choi [2], Masuda et al. [3] and Lee et al. [4] that limits of conventional solid particle suspensions can be broken down, considering the notion of nanoparticle fluid suspensions. The nanometer sized

particles like metallic oxides, carbide ceramics, ceramics, metals, nitride, semiconductors, carbon nanotubes or alloyed nanoparticles dispersed in the base fluids like oil, water or ethylene glycol forms. This nanoparticle fluid amalgamation is known as nanofluid.

Nanoparticles are basic forming components of nanofluids so pace of research on nanofluids has increased due to the reason of the advancement of nanotechnology in general and accessibility of nanoparticles specifically. Nanoparticles have higher surface area to volume ratio as compared to micro-sized particles, reason is occupancy of large number of atoms on boundaries which gives them high stability in suspensions. Consequently high thermal conductivity is shown by nano suspensions probably due to increased convection between liquid surfaces and solid particles. Nanofluids show augmentation in their properties like thermal conduction. The characteristics like increased stability and higher conductivity of the scattered 'Nano-species' make them highly desirable for designing heat transit fluids. The suspensions having smaller quantity of nano-particles and possessing high stability, these can help in future with designing efficient thermal management systems. As various industrial products such as power electronic circuits, car engines, computers, high power lasers, x-ray generators etc. require cooling for better and reliable performance.

The hybrid nanofluids possessing more than a single kind of nanoparticles, have emerged encompassing more thermal conductivity as compare to nanofluids. The researchers are focused in recent years to develop hybrid nanofluids which should be more stable with extra sustainability, having less viscosity and have higher thermal conduction. These fluids have revolutionized variety of heat transfer functions like cooling, nuclear systems, electronics, automobile radiators, in machining, generators, lubrication, solar heating, welding, thermal storage, heating in buildings, drug reduction, biomedical, refrigeration and in the sector of defense etc. Therefore, these kind of industrial applications require the stable and new production techniques for hybrid nanofluids by using less expensive equipment.

Nickel Zinc ferrites are technologically significant nanoparticles possessing proper-

ties such as higher electrical resistivity, increased mechanical strength, better magnetic permeability, low dielectric loss and good chemical stability. Nickel Zinc ferrites have various applications in electromagnetic equipments like in data storage devices, inductors, actuators, magnetic sensors, medical diagnosis, targeted drug delivery and in electromagnetic wave absorbers. The electronic gadgetry requires these materials having customized compression for out sizing the shape with requisite thickness, the process can be hard if particles are of larger size. Quite a few procedures like precipitation, ball milling and hydrothermal, have been recommended for acquirement of Nickel Zinc ferrite. The ferro/ferri-magnetic nanoparticles suspended in hauler fluids (electrically insulated) are recognized as ferrofluids which is a type of colloidal fluid. Investigation regarding ferronano-liquids (Fe_2O_3 and ethylene) with shear thinning behavior is studied by Gallego et al. [5].

In situations where the heat transfer is forecasted, it is crucial to analyze thermal stratification.The variations in temperature and difference in fluid densities are reasons for thermal stratification which causes free convection of heat transfer in numerous engineering and industrial processes. Batteries which are very large can have self-discharging or internal leakages due to thermal stratification. It is essential to have absolute understanding regarding nuclear reactor's design with respect to thermal stratification as it can cause any mishap in reactor. Such situations can be avoided through better stratification and in many energy procedures high energy efficiency is achievable.

Thermal radiation, the only mechanism for heat transfer in vacuum, is a process of heat energy emission from radiated surface in the form of electromagnetic waves in all directions. This process is very much effective in generating high temperature. Thermal radiation is important in the fields of physics and engineering due to its critical effect on various fluid flows and heat transfer processes. Space technology has also been benefited by the role of thermal radiation which has made possible the manufacturing of devices with finest thermal efficiency being operated at enormously high temperatures. The scientists have developed interest in the boundary layer flows along with heat trans-

fer due to stretching surface because this phenomenon has innumerable applications in manufacturing industrial procedures i.e., in electro-chemistry, tinning, chemical waste migration, annealing of copper wires, metal spinning, hot rolling, artificial fiber and in paper production.

Generally, at boundary the velocity of fluid is considered insignificant and taken zero but at nano scale the dynamics of fluids make it compulsive regarding such velocity which is termed as slip velocity. Consequently, the various slip velocity models have been proposed. Flow behavior with no-slip conditions (body and fluid particles posses matching velocity), is examined by many researchers. Slip boundary condition characterizes the behavior of fluid's flow in nano/micro systems such as micro valve, nozzles, pumps and hard drive. Furthermore, it is used for polishing synthetic heart valves and inner cavities. Aforesaid practical applicability has prompted the focus of researchers to analyze the flow and heat transfer at micro level in relation to slip effects.

1.2 Literature Review

Thermal conduction is low in base fluids like oil, ethylene glycol, kerosene and water which is also a hindrance in heat transfer procedures. Nanoparticles in small quantity *i.e.,* under one percent are suspended in the base fluid for the purpose of increment in thermal conduction and due to this increment, the heat transfer properties are doubled. There are various features of nanoparticles which affect the thermal conductivity such as size and shape, volume fraction, temperature and nature of particle material. Nanoparticles in essence are metal or oxides possessing distinctive chemical and physical properties. Choi et al. [2] through ground breaking research has pioneered the enhancement of thermal qualities of fluids by adding the nanoparticles. Practically the latest type of nanofluids identified as hybrid nanofluids possess variety of applications in various fields such as manufacturing, transportation, medical, defense and acoustics etc. The appropriate dispersion of hybrid nanoparticles causes remarkable enhancement

in thermal conductivity. Nanofluids are famous for heat transfer qualities in contrast to usual fluids, moreover introduction of hybrid nanofluids have improvised these qualities. Utilizing numerical technique Hayat and Nadeem [6] examined the heat transfer qualities for boundary layer flow of three-dimensional rotating hybrid nanofluid over a stretching sheet with heat generation, radiation and chemical reaction effects. Nadeem et al. [7] investigated the properties of 3D stagnation point flow of hybrid nanofluid passing a circular cylinder and compared the results of higher heat transfer rate in hybrid nanofluids and nanofluids.

Nanoparticles possess capabilities that increase the heat transfer process and thermal conductivity of base fluid. The addition of ferrite nanoparticles into the base liquid notably enhances the heat transfer and thermal conductivity. There are many worth mentioning examples of heat transfer such as avionics cooling systems and cooling/heating system of buildings *etc.* The large surface area of nanoparticles in comparison to micrometer-sized particles, qualify them with unmatched heat transfer qualities [8]. The utilization of Nikel Zinc ferrite can be seen in electromagnetic applications with higher permeability like in inductors and electromagnetic wave absorbers. Many researchers have recommended that using Nickel Zinc nanoparticles energy losses associated to bulk powders can be minimized [9-11]. In this research ethylene glycol ($C_2H_6O_2$) is taken as base fluid and Nickel Zinc ferrite ($NiZnFe_2O_4$) as nanoparticles. Usually inverted spinals at room temperature are ferro-magnetic and normal spinals are paramagnetic. Furthermore, at low temperature in nature zinc ferrits show anti-ferromagnetic behavior. The aforesaid aspect has increased relevance of ferro-magnetic nanofluids applications in actual world [12-13]. Neuringer [14] analyzed ferro-fluid flow considering the impact of thermal gradient and magnetic field . The phenomenon of heat transfer in the flow of ferro-magnetic fluid is examined by Majeed et al. [15]. The flow of hybrid nanofluid over curved surface with entropy optimization coating and nonlinear thermal radiation is analyzed by Lu et al. [16]. Convective heat along with mass flux boundary conditions supported this analysis. Transfer of heat, an observable fact in ferro-magnetic nanofluids

is investigated by Muhammad and Nadeem [17]. Furthermore, comparison is drawn for various ferrite nanoparticles during the analysis of heat transfer rate, temperature field, axial velocity and wall shear stress. The flow of Williamson ferro-fluid under the influence of magnetic dipole, viscous dissipation and radiation past a stretchable sheet is examined by Hayat et al. [18]

Numerous industrial and engineering areas e.g., crystal growing, hot rolling, glass blowing, rubber sheet manufacturing, paper production, annealing of copper wires and so on, involve the applications of fluid flow over stretched surfaces. Initially, the fluid flow over linearly stretching surface is studied by Crane [19] and his study encouraged the researchers for further findings. Gupta and Gupta [20] carried out an extraordinary research work on fluid flow over a spongy surface. Hydro-magnetic flow over stretched surface is reported by Chakrabarti and Gupta [21]. Fluid flow in accordance to Power law passing over a linearly stretched surface, under the influence of magnetic force is studied by Andersson et al. [22]. Hayat et al. [23] worked on Oldroyd-B fluid flow having effects of heat source. Flow of a nanofluid with elastic and viscous properties, over bi-directional stretched surface with Newtonian heating effect is illustrated by Ramzan and Yousaf [24]. Jeffrey nanofluid flow is examined by Hussain et al. [25] using exponentially stretched surface considering effects of radiation.

The curved stretching, in modernized engineering technologies has enormous significance and applications *e.g.*, in transportation sector and electronics. Numerical solution is calculated by Sanni et al. [26] for viscous liquid flow over nonlinearly curved stretched channel. The numerical investigation of MHD nanoliquid flow along with the heat transit over nonlinearly stretched curved sheet is conducted by Sharma et al. [27]. Afridi et al. [28] using second law analyzed heat transfer with influences of magnetic field, dissipation and entropy production in nanoliquid flow past a curved stretching sheet. Ferro-fluid flow via an extended curved surface is demonstrated by Sajid et al. [29] considering the magnetic forces and Joule heating. The time dependent fluid flow through a curved spongy sheet is analyzed by Rosca and Pop [30].

Latest researches have focused on qualities of nanofluids and conventional liquids flow over stretched surfaces with consideration to thermal radiation and heat transfer. Heat transfer of micropolar fluid with the effects of thermal radiation over a curved surface is analyzed by Naveed et al. [31]. The MHD mixed convection flow of nanoliquid in existence of nonlinear radiation past a linearly stretchable curved sheet is studied by Hayat et al. [32]. Hayat et al.[33] examined fluid flow through curved stretchable sheet with double stratification, Joule heating and thermal radiation. Nadeem et al.[34] examined the carbon nanotubes effects in magneto nanofluid with variable viscosity flow past a curved stretching surface. Dual solutions are given by Reddy et al. [35] for the nonlinear radiative nanofluid flow through a curved stretching surface. The Carbon nanotube based nanofluid flow over stretched curved sheet is studied by Saba et al. [36] and focused on heat transfer through radiative flow and heat generation. Soomro et al. [37] analyzed the influence of thermal radiation and velocity slip on the nanofluid flow, also focused on heat transfer of magneto-hydrodynamic (MHD) stagnation-point nanofluid flow through horizontal linearly stretching sheet. Homotopy Analysis method (HAM) is adopted by Ahmad et al. [38] for investigating slips analysis of squeezed Newtonian fluid with mass and heat flow via porous medium with double stratification. The slip flow analysis of nanoliquid flow through nonlinear permeable surface is carried out by Rana et al. [39], considering thermal radiation and varying magnetic field. The radiation effects for a nanofluid past a curved stretching surface is studied by Abbas el al. [40], in th of uniform magnetic field by incorporating slip effect and combined effects of heat generation and radiation. Koriko et al. [41] studied investigated the radiative Micropolar fluid flow over a thermal stratified vertical sheet in influence of dual stratification. Muhammad et al. [42] studied the phenomenon of stratification in Casson fluid flow over the vertical stretching cylinder considering slip effects in the region of stagnation point. They also investigated the mass and heat transfer with chemical and thermal effects in this flow. Flow of ferro-magnetic fluid with effect thermal stratification past a stretching sheet is argued by Muhammad et al. [43]. Rehman et al. [44] discussed the flow of Eyring-Powell

fluid passing through inclined stretching cylinder considering effect of dual stratification with mixed convection. Linear thermal radiation and slip effect on nano fluid passing through a stretching cylinder with dual stratification is studied by Hayat et al. [45].

The current study is prompted by cited work as mentioned above and is discoursed for examining the effects on flow and heat transit of hybrid nanofluid flow past a curved surface with velocity slip, thermal stratification and nonlinear radiation. Such study is not yet conducted according to the best of our knowledge. All results presented through graphs and tables are comprehensively analyzed.

Chapter 2

Preliminaries

Elementary definitions, concepts and fundamental laws are stated in this chapter, which are useful in understanding the work in the third and fourth chapters.

2.1 Fluid

Fluid is a substance which has ability to flow smoothly and constantly. Some examples are mercury, shampoos, cooking oil, blood and oxygen.

2.2 Fluid mechanics

It is the class of natural science that deals with the behavior of fluid flow and forces of the fluid. It is futher classified into two classes.

2.2.1 Fluid statics

It is the class of fluid mechanics which explores the aspects of liquid in stationary state.

2.2.2 Fluid dynamics

The class of fluid mechanics which explores the aspects of fluid in motion state.

2.3 Flow

Flow is described as a material in which deformation in smoothly and continuously under the influence of various forces, flow is further divided into two main subclasses.

2.3.1 Laminar flow

A flow of fluid in regular paths without interruption between layers is known as laminar flow.

2.3.2 Turbulent flow:

Turbulent flow is the phenomenon in flow field where fluid has irregular paths between layers.

2.4 Stress

Within the deformable body, the force per unit area is identified as stress. It's unit in SI is Nm^{-2} and dimension $\left[\frac{M}{LT^2}\right]$. Mathematically,

$$\tau_{ji} = \frac{F_i}{A_j} \qquad i, j = x, r, \tag{2.1}$$

where the componants of force and area are F_i, A_j respectively. Stress has two subdivisions:

2.4.1 Shear stress

The force is identified as Shear stress, if it is acting on a substance parallel to the unit area of the surface.

2.4.2 Normal stress

The force is identified as Normal stress, if it is acting on a substance perpendicular to the unit area of the surface.

2.5 Viscosity

It is the attribute of fluid resistance to flow in the presence of various forces is known as viscosity. Its mathematical denotation is given as:

$$\text{viscosity} = \frac{\text{shearstress}}{\text{gradient of velocity}}. \tag{2.2}$$

2.5.1 Dynamic viscosity

It is the specific resistive fluid property against external force/ deformation. It is denoted by μ and it's is unit Nsm^{-2}.

2.5.2 Kinematic viscosity

It is the kind of viscosity which is measured in the presence gravity and density. Mathematically denoted as:

$$v = \frac{\mu}{\rho}. \tag{2.3}$$

In SI system, its unit is m^2s^{-1}.

2.6 Newton's law of viscosity

Fluids which demonstrate the continuous and direct relation amid shear stress and gradient of velocity. Mathematically, expression for Newtons law can be represented as:

$$\tau_{rx} \propto \frac{du}{dr}, \tag{2.4}$$

or

$$\tau_{rx} = \mu \left(\frac{du}{dr} \right), \tag{2.5}$$

in which τ_{rx} indicate the shear force applied on the fluid's element and μ indicate the proportionality constant.

2.7 Newtonian fluids

Satisfaction of Newton's law of viscosity by the fluids like water, alcohol, glycerin and kerosene, with the value of μ is constant are identified as Newtonian fluids. Such liquids have shear force (τ_{rx}) direct relation to the gradient of velocity $\left(\frac{du}{dr}\right)$.

2.8 Non-Newtonian fluids

These are fluids like yogurt, honey and mayonnaise which disobey Newton's viscosity law, with nonlinear and direct relationship connecting gradient of velocity with shear stress. Mathematical denotation in the case is given as:

$$\boldsymbol{\tau}_{rx} \propto \left(\frac{du}{dr} \right)^{n}, \ n \neq 1, \tag{2.6}$$

or

$$\boldsymbol{\tau}_{rx} = \eta_1 \frac{du}{dr}, \ \eta_1 = s \left(\frac{du}{dr} \right)^{n-1}. \tag{2.7}$$

For $n = 1$, Eq. (2.7) represents the Newton's law of viscosity.

2.9 Nanofluid

A liquid having smallest particles (nanometer particles) is referred as Nanofluid, formed by the nano sized particles colloidal suspensions in the conventional fluid. The metals, oxides and nanotubes are typically examples of nanoparticles with water and oil as regular base fluids.

2.10 Density

The ratio of mass of a subtance to its volum are recognized as Density. Commonly, it measures stuff of a substance there in a unit volume.

Mathematical denotation as follows:

$$\rho = \frac{M^*}{V^*}. \tag{2.8}$$

In SI system units it is calculated as kgm^{-3}.

2.11 Pressure

The force exerted on a surface per unit area, recognized as Pressure. Mathematically, it is denoted as:

$$P = \frac{F_1}{A}. \tag{2.9}$$

The SI unit of pressure is Nm^{-2}.

2.12 Mechanism of heat flow

The form of energy flow from hotter to colder area is called heat flow which happens involving two objects of different temperatures via one of the three following ways:

2.12.1 Conduction

The process of heat movement in liquids and solids from warmer to cooler areas due to collision of free electrons and molecules is recognized as conduction. Moreover, this do not involves movement of molecules for heat transfer. Denoted mathematically as:

$$\frac{\boldsymbol{q}}{A} = k^* \left(\frac{T_a - T_b}{X_a - X_b} \right) = k^* \frac{\Delta T}{\Delta X}, \tag{2.10}$$

where

$$\boldsymbol{q} = -k^* A \frac{dT}{dx}. \tag{2.11}$$

Here, T_a (temperature) is greater than T_b, temperature gradient is represented as $\frac{dT}{dx}$ and heat conduction from higher to lower indicated with minus sign.

2.12.2 Radiation

The occurrence of heat flow from hotter to colder region due to electro-magnetic waves is known as radiation. It plays crucial function during heat transfer in vacuum and mathematically denoted as:

$$\boldsymbol{q}_r = e\overline{\sigma} A \left(\Delta T \right)^4. \tag{2.12}$$

2.12.3 Convection

The movement of molecules in liquids and gases transferring heat from hotter to cooler region is identified as convection which is mathematically symbolized as:

$$q_c = h^* A \left(T_s - T_\infty \right). \tag{2.13}$$

2.13 Convective boundary condition

This condition also known as Robin's boundary condition, is defined on the surface that both heat conduction and heat convection at the sheet are equal and in the same direction. Its mathematical denotation is as:

$$k^* \left(\frac{\partial T}{\partial m} \right)_x = h^* [T_f(x,t) - T_w(x,t)]. \tag{2.14}$$

2.14 Slip condition

The difference in velocities of fluid particles and the body is identified as slip condition. In Slip condition similar to the symmetry condition the fluid velocity is not influenced by the wall in planes parallel and close to the wall. Navier [46] was the first to coin the term slip condition in his Slip Velocity Model, which is proportional to the shear stress experienced by the fluid continuous at the solid wall.

$$U \infty \tau,$$

$$U = L\tau. \tag{2.15}$$

Here, L is slip length and if length is zero then there is no slip.

2.15 Stratification

The phenomenon of particles deposition into layers under effect of temperature change and mixture of various fluids having different densities, is recognized as Stratification. The importance of stratification is well recognized in convective transport mechanism reasoned to its extensive applications in industrial, natural and engineering fields.

2.15.1 Thermal stratification

Thermal stratification arises due to variation in temperature which augments the density variation in the fluid medium. The fluid expands and contracts during heating and cooling which cause variation in density. The fluid stratification due to the variation in the temperature caused by radiating heated sheet e.g, a vertical plate, and curved sheet etc.

2.16 Entropy

Entropy is defined as the measurement of thermal energy per unit temperature in the system due to molecular disorder or randomness in the system.

2.17 Non-dimensional numbers

2.17.1 Reynolds number (Re)

The inertial forces divided by viscous forces is known as Reynolds number which is a convenient parameter to predict laminar or turbulent flow condition. Mathematical denotation of this number is given as:

$$\begin{aligned} \mathrm{Re}_x &= \frac{\text{inertial forces}}{\text{viscous forces}}, \\ &= \frac{U_W \times L^*}{\upsilon}. \end{aligned} \tag{2.16}$$

Reynolds number (Re_x) within a same fluid, are used for explaining the distinctive behavior of flow (laminar or turbulent flow). Laminar flow takes place at small Reynolds number ($\mathrm{Re}_x < 2000$), causing prominent viscous effects. High Reynolds number ($\mathrm{Re}_x > 4000$) are noted in turbulent flow, having prominent inertial effects.

2.17.2 Hartmann number (M)

The ratio of electro-magnetic force to viscous force is identified as Hartmann number or megnetic peremeter(M). Mathematical representation is given by:

$$M = \beta_0 L^* \sqrt{\frac{\sigma^*}{\mu}}. \tag{2.17}$$

2.17.3 Radius of curvature parameter (k_c)

It is the radius of the given circle at a point where it joins the curve with uniform tangent and curvature.

2.17.4 Prandtl number (Pr)

The computation of heat transfer between solid body and flowing fluid via a dimensionless parameter and is mathematically denoted as;

$$\mathrm{Pr} = \frac{\upsilon}{\alpha^*}, \tag{2.18}$$

$$= \frac{\mu C_p}{k^*}, \tag{2.19}$$

where $\alpha^* = \frac{k^*}{(\rho C_p)}$ and $\upsilon = \frac{\mu}{\rho}$.

2.17.5 Radiation parameter (Ra)

This is the characterized as relative assistance of conduction to the transmission of thermal radiation. It is symbolized as follows:

$$Ra = \frac{4\overline{\sigma} T_\infty^3}{k^* \overline{k}}. \tag{2.20}$$

2.17.6 Biot number (Bi)

It is the ratio of resistances inside and at surface of a body against heat transfer. Mathematical representation is as below:

$$Bi = \frac{h^* L^*}{k^*}. \tag{2.21}$$

2.17.7 Schmidt number (Sc)

Ratio of non-Newtonian viscosity (kinematic) to mass diffusivity is known as Schmidt number. Mathematically

$$Sc = \frac{\upsilon}{D_B}. \tag{2.22}$$

2.17.8 Skin friction coefficient (C_{fx})

The drag between liquid and solid surface, experienced by a liquid during flow over a surface, is identified as Skin friction coefficient also causing decline in the rate of flow. Mathematical denotation is shown as below:

$$C_{fx} = \frac{\tau_{rx}}{\frac{1}{2}\rho U_W^2}. \tag{2.23}$$

2.17.9 Nusselt number (Nu_L)

It is a dimensionless amount that corresponds to convection and conduction heat transit parameters at the boundary. Mathematically shown as:

$$Nu_L = \frac{h^* \Delta T}{k^* \Delta T/l} = \frac{h^* L^*}{k^*}. \tag{2.24}$$

2.18 Conservation laws

These are the laws which deal with the conserved quantity, a quantity which can be calculated and remains unaffected over a period of time in an isolated system. The conservation laws, used for flow specification in the sub-sequential analysis are specified below.

2.18.1 Mass conservation law

The phenomenon in which entire mass stay preserved in a closed system is called Conservation law for mass having mathematical symbolization as below:

$$\frac{D\rho}{Dt} + \rho \boldsymbol{\nabla}.\mathbf{U} = 0, \tag{2.25}$$

or

$$\frac{\partial \rho}{\partial t} + (\mathbf{U}.\boldsymbol{\nabla})\,\rho + \rho \boldsymbol{\nabla}.\mathbf{U} = 0, \tag{2.26}$$

or

$$\frac{\partial \rho}{\partial t} + \boldsymbol{\nabla}.\,(\rho \mathbf{U}) = 0. \tag{2.27}$$

In foregoing is the equation of continuity. Below is the equation (2.28) for steady flow:

$$\boldsymbol{\nabla}.\,(\rho \mathbf{U}) = 0. \tag{2.28}$$

Moreover, equation for incompressible fluid is expressed as:

$$\boldsymbol{\nabla}.\mathbf{U} = 0. \tag{2.29}$$

2.18.2 Momentum conservation law

It is termed as the total linear momentum remains constant in a closed system and mentioned as:

$$\rho\frac{D\mathbf{U}}{Dt}=\operatorname{div}\boldsymbol{\tau}+\rho\mathbf{b}, \tag{2.30}$$

where $\mathbf{b}$ is the body forces and Cauchy stress tensor (τ) is symbolized as:

$$\boldsymbol{\tau}=-\mathbf{pI}+\mathbf{S}. \tag{2.31}$$

The equation for incompressible fluid is denoted by:

$$\rho\left(\frac{\partial\mathbf{U}}{\partial t}+(\mathbf{U}.\boldsymbol{\nabla})\mathbf{U}\right)=-\boldsymbol{\nabla}\mathbf{p}+\mu\boldsymbol{\nabla}^2\mathbf{U}+\rho\mathbf{b}. \tag{2.32}$$

Futher, equation for steady flow is given as:

$$\rho(\mathbf{U}.\boldsymbol{\nabla})\mathbf{U}=-\boldsymbol{\nabla}\mathbf{p}+\mu\boldsymbol{\nabla}^2\mathbf{U}+\rho\mathbf{b}. \tag{2.33}$$

2.18.3 Law of energy conservation

It is known as energy equation which is explicated as whole energy is preserved in the closed system.

$$(\rho C_p)\frac{D\mathbf{T}}{Dt}=\boldsymbol{\tau}.\mathbf{L}-\operatorname{div}\mathbf{q}+\rho\mathbf{r}, \tag{2.34}$$

where the $\mathbf{r}$ is the dissipation effect, $\mathbf{L}=\boldsymbol{\nabla}\mathbf{V}$ and thermal diffusion $\boldsymbol{q}=-k\boldsymbol{\nabla}\boldsymbol{T}$ by Fourier's law. Moreover, the equation for steady flow is below:

$$(\rho C_p)(\mathbf{U}.\boldsymbol{\nabla})\mathbf{T}=k\boldsymbol{\nabla}^2\mathbf{T}+\rho. \tag{2.35}$$

2.18.4 Law of conservation of concentration

The volume fraction equation for nanoparticles is

$$\frac{\partial \mathbf{C}}{\partial t} + \mathbf{U}.\boldsymbol{\nabla}\mathbf{C} = -\frac{1}{\rho}\boldsymbol{\nabla}.\mathbf{j}_p. \tag{2.36}$$

The mass diffusion j_p by the Fick's law is

$$\mathbf{j}_p = -\boldsymbol{\rho}\mathbf{D}_B\boldsymbol{\nabla}\mathbf{C}. \tag{2.37}$$

From equations (2.36) and (2.37), we have

$$\frac{\partial \mathbf{C}}{\partial t} + \mathbf{U}.\boldsymbol{\nabla}\mathbf{C} = \mathbf{D}_B\boldsymbol{\nabla}^2\mathbf{C}\ , \tag{2.38}$$

Futhermore, equation for time independent flow is as following

$$\mathbf{U}.\boldsymbol{\nabla}\mathbf{C} = \mathbf{D}_B\boldsymbol{\nabla}^2\mathbf{C}\ . \tag{2.39}$$

2.19 Thermal diffusivity

It is the ratio of thermal conductivity to specific heat capacity and density and mathematically shown as:

$$\alpha^* = \frac{k^*}{\rho C_p}. \tag{2.40}$$

2.20 Thermal conductivity

It is the measurement of the capacity of substance to conductive heat. The Fourier law of heat conduction with below symbolization, is the rate of the product of heat transit amount (q) through a meterials thickness (d^*) to the area (A) and unit temperature difference (ΔT).

$$k = \frac{qd^*}{A(\Delta T)}. \tag{2.41}$$

$Wm^{-1}K^{-1}$ is the thermal conductivity unit in SI system.

Chapter 3

Impact of nonlinear thermal radiation and entropy optimization coatings with hybrid nanofluid flow past a curved stretched surface

3.1 Mathematical formulation

Consider a time independent 2D, isochoric and hybrid nanofluid flow past a stretchable curved surface in the form of circle with convective heat and mass flux conditions. Here, to some extent curved surface a higher value of $\overline{R}$ is associated. The linearly stretched velocity is taken as $U_W = Sx$ in the x-direction. A magnetic field is applied normal to the fluid flow. The electric and induced magnetic fields are disregarded due to our supposition of small Reynolds number (Figure 3.1).

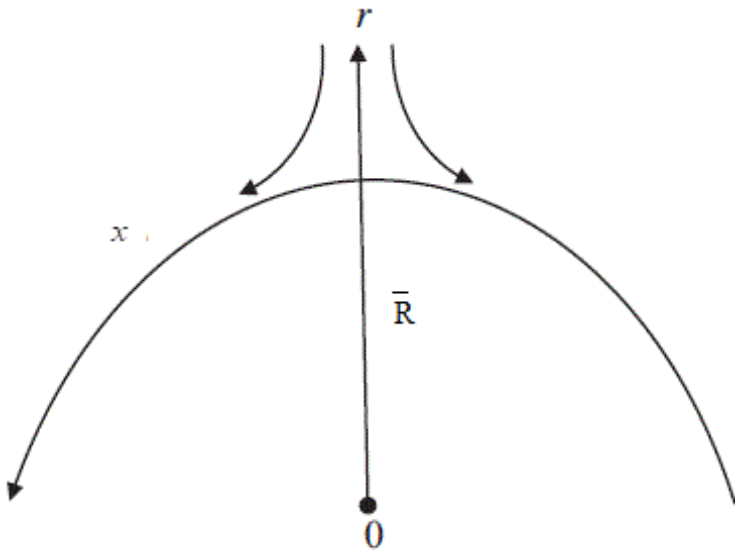

Figure 3.1 : Flow geometry of the mathematical model for a curved surface

The subsequent equations govern the assumed system:

$$((r+\overline{R})V))_r + \overline{R}Ux = 0, \tag{3.1}$$

$$p_r = \frac{\rho_{nf}}{r+\overline{R}}U^2, \tag{3.2}$$

$$VU_r + \frac{\overline{R}}{r+\overline{R}}UU_x + \frac{1}{r+\overline{R}}UV = -\frac{\overline{R}}{(r+\overline{R})\rho_{nf}}p_x + \frac{\mu_{nf}}{\rho_{nf}}(U_{rr} + \frac{1}{r+\overline{R}}U_r$$
$$-\frac{1}{(r+\overline{R})^2}U) - \sigma^*\frac{\beta_0^2}{\rho_{nf}}U, \tag{3.3}$$

$$VT_r + \frac{\overline{R}}{(r+\overline{R})}T_x = \alpha(T_{rr} + \frac{1}{r+\overline{R}}T_r - \frac{Q^*}{(\rho C_{p)_{nf}}}(T_\infty - T)$$

$$+\frac{1}{(r+\overline{R})(\rho C_p)_{nf}}((r+\overline{R})q_r)_r, \tag{3.4}$$

$$VC_r + \frac{\overline{R}}{r+\overline{R}}UC_x = D_B(C_{rr} + \frac{1}{r+\overline{R}}C_r). \tag{3.5}$$

The subsequent boundary conditions support the governing equations $(3.1) - (3.5)$

$$V = 0, U = U_W(x) = Sx, -k_f T_r = h\left(T_f - T\right),$$

$$-D_B C_r = J_W \text{ at r} = 0,$$

$$U \to 0, U_r \to 0, T \to T_\infty, C \to C_\infty \text{ as } r \to \infty. \tag{3.6}$$

The Thermo phyiscal characteristics of the hybrid nano-liquid are mentioned in Table 3.1.

Table 3.1 : Ethylene glycol($C_2H_6O_2$) and Nickel-zinc ferrite ($NiZnFe_2O_4$) having the values of ρ (density),k (themal conductivity) and C_p (heat capacity) [47-52] .

Thermo physical properties	Ethylene glycol	Nickel-zinc ferrite
$C_p(Jkg^{-1}\,k^{-1})$	2382.0	710.0
$k\ (Wm^{-1}K^{-1})$	0.2490	6.3
$\rho\ (kgm^{-3})$	1116.6	4800.0
Pr	204.0	–

These properties are represented in the mathematical form as:

$$\mu_{nf} = \mu_f(1-\psi)^{-2.5},\ \alpha = \frac{k_{nf}}{(\rho C_p)_{nf}}, \tag{3.7}$$

$$\frac{\rho_{nf}}{\rho_f} = (1-\psi) + \psi\frac{\rho_s}{\rho_f},\ \frac{(\rho C_p)_{nf}}{(\rho C_p)_f} = (1-\psi) + \psi\frac{(\rho C_p)_s}{(\rho C_p)_f}, \tag{3.8}$$

$$\frac{k_{nf}}{k_f} = \frac{2\psi(k_f - k_s) + (2k_f + k_s)}{\psi(k_f - k_s) - (2k_f - k_s)}. \tag{3.9}$$

Nonlinear radiation heat-flux (under Rosseland's approximation) used in equation (3.4), is given by:

$$q_r = \frac{4\overline{\sigma}}{3\overline{K}}(T^4)_r = \frac{16\overline{\sigma}}{3\overline{K}}T^3T_r.$$

Here, the subsequent dimensionless transformation are used :

$$\xi = (\frac{S}{\upsilon_f})^{\frac{1}{2}}r,\ p = \rho_f S^2x^2P(\xi),\ T = T_\infty(1+(\Theta_W-1)\Theta),$$

$$C = C_\infty + \frac{J_W}{D_B}(\frac{\upsilon_f}{S})^{\frac{1}{2}}\Phi(\xi),\ U = SxF'(\xi)\ ,\ V = \frac{-\overline{R}}{r+\overline{R}}(S\upsilon_f)^{\frac{1}{2}}F(\xi)\,. \tag{3.10}$$

Here, the superscript ($'$) indicates the derivative w.r.t ξ , and $\Theta_W = \frac{T_f}{T_\infty}$. The above tranformations (3.10) satisfy that equation (3.1) is inevitable. However, equations $(3.2)-(3.6)$ reduce to:

$$P' = (1-\psi+\psi\frac{\rho_s}{\rho_f})\frac{F'}{\xi-k_c}, \tag{3.11}$$

$$\frac{2k_c}{\xi+k_c}P = (1-\psi+\psi\frac{\rho_s}{\rho_f})(\frac{k_c}{(\xi+k_c)^2}FF' + \frac{k_c}{\xi+k_c}(FF''-F'^2) - MF')$$
$$+(1-\psi)^{-2.5}(F''' + \frac{1}{(\xi+kc)}F'' - \frac{1}{(\xi+kc)^2}F'''), \tag{3.12}$$

$$\frac{1}{\mathrm{Pr}}(\frac{k_{nf}}{k_f} + R_a(1+(\Theta_W-1)\,\Theta)^3)(\Theta'' + \frac{1}{\xi+k_c}\Theta') + (1-\psi+\psi\frac{(\rho C_p)_s}{(\rho C_p)_f})\frac{k_c}{\xi+k_c}F\Theta'$$
$$+\lambda^*\Theta + \frac{3R_a}{\mathrm{Pr}}(1+(\Theta_W-1)\,\Theta)^2\,(\Theta_W-1)\,\Theta'^2 = 0, \tag{3.13}$$

$$\Phi'' + \frac{1}{\xi+k_c}\Phi' + S_c\left(\frac{k_c}{\xi+k_c}\right)F\Phi' = 0, \tag{3.14}$$

$$F(0) = 0,\ F'(0) = 1,\ \Theta'(0) = -Bi(1-\Theta\,(0)),\ \Phi'(0) = -1,$$

$$F'(\infty)\to 0,\ F''(\infty)\to 0,\ \Theta\,(\infty)\to 0,\ \Phi(\infty)\to 0. \tag{3.15}$$

Eliminating the pressure term $P(\xi)$ by solving equations (3.11) and (3.12), resulting

in the following equation:

$$F^{iv}+\frac{2}{\xi+k_c}F'''-\frac{1}{(\xi+k_c)^2}F''+\frac{1}{(\xi+k_c)^3}F'+(1-\psi)^{2.5}\left(1-\psi+\psi\frac{\rho_s}{\rho_f}\right)\{\frac{k_c}{\xi+k_c}(FF'''+F'F'')$$

$$-\frac{k_c}{(\xi+k_c)^2}\left(F'^2-FF''\right)-\frac{k_c}{(\xi+k_c)^3}FF'\}-(1-\psi)^{2.5}M\left(\frac{1}{\xi+k_c}F'+F''\right)=0, \quad (3.16)$$

with

$$k_c=\overline{R}\left(\frac{S}{\upsilon_f}\right)^{\frac{1}{2}},\ Bi=\frac{h}{k_f}\left(\frac{S}{\upsilon_f}\right),\ S_c=\frac{\upsilon_f}{D_B},\ M=\sigma^*\frac{\beta_0^2}{\rho_f S},$$

$$\Pr=\frac{\upsilon_f}{\alpha^*},\ \lambda^*=\frac{Q^*}{S(\rho C_p)_f},\ R_a=\frac{16\overline{\sigma}}{3k_f\overline{k}}T_\infty^3. \quad (3.17)$$

Mathematical expressions for surface drag force coefficient (C_{fx}), Sherwood number (Sh_x) and Nusselt number (Nu_x) defined as:

$$C_{fx}=\frac{2\tau_{rx}}{\rho_f U_W^2},\ Nu_x=\frac{xq_w}{k_f(T_f-T_\infty)},\ Sh_x=-\frac{x}{C-C_\infty}C_r, \quad (3.18)$$

where

$$\tau_{rx}=\mu_{nf}\left(U_r-\frac{1}{r+\overline{R}}U\right)_{r=0},\ q_w=-\left((q_r)+T_r\right)_{r=0}. \quad (3.19)$$

The transformations (3.10) and (3.19), formulate equation (3.18) as:

$$(\mathrm{Re}_x)^{0.5}C_{fx}=(1-\psi)^{-2.5}\left(F''(0)+\frac{F'(0)}{k_c}\right), \quad (3.20)$$

$$(\mathrm{Re}_x)^{-0.5}Nu_x=-[\frac{k_{nf}}{k_f}+Ra(1+(\Theta_W-1)\Theta(0))^3]\Theta'(0), \quad (3.21)$$

$$(\mathrm{Re}_x)^{-0.5}Sh_x=\frac{1}{\Phi(0)}. \quad (3.22)$$

Reynolds number is given as:

$$Re_x=\frac{U_W}{\upsilon_f}x. \quad (3.23)$$

Dimensional form of the equation of entropy generation is [53]

$$E_G = \frac{k_{nf}}{T_f^2}\left[\left(1+\frac{16\overline{\sigma}T^3}{3k_{nf}\overline{k}}\right)(T_r)^2\right] + \frac{\mu_{nf}}{T_f}(U_r)^2 + \frac{\sigma^*}{T_f}\beta_0^2U^2 + \frac{RD}{C_\infty}(C_r)^2 + \frac{RD}{T_f}C_rT_r, \quad (3.24)$$

After application of suited transformations, the changed form of equation (3.24) is as under:

$$N_g = \frac{E_G}{E_0} = \mathrm{R}e_x\left[Ra(1+\Sigma\Theta)^3 + \frac{k_{nf}}{k_f}\right]\Theta'^2 + \frac{Br\mathrm{R}e_x}{\Sigma^2}F''^2 + \frac{Br\mathrm{R}e_x}{\Sigma^2}F'^2$$

$$+\frac{\Omega\mathrm{R}e_x}{\Sigma}\left(\Phi'^2 + \frac{\Theta'\Phi'}{\Omega}\right), \quad (3.25)$$

These Brinkman number, constant parameter and temperature difference are given in the subsequent form:

$$Br = \frac{\mu_{nf}U_W^2}{k_{nf}T_f},\ \Sigma = \Theta_W - 1,\ \Omega = \frac{C_\infty RD}{k_{nf}}. \quad (3.26)$$

3.2 Results and discussion

Numerical solution is integrated, for the system of equations (3.13), (3.14) and (3.16) with boundary condition (3.15). All the results are obtained by using numerous fixed values of $M = \psi = 0.1$, $Sc = \Theta_W = Ra = \lambda^* = 0.5$ and $k_c = \mathrm{Pr} = 10$ graphically, by utilizing the MATLAB built-in function ($bvp4c$). Intended for this procedure, firstly the differential equations with the higher order to the equations of order one are changed by utilizing novel variables. The boundary condition (3.15) along with the solution needs to be satisfied by the presumptions.

Table 3.2, illustrates the validation of the presented results, observing an exceptional concurrence with Sanni et al. [26] when $m = 1$, $\psi = 0.0$, and in the dearth of temperature and concentration profile. Observing the impression of ψ , on temperature and velocity distributions, Figures 3.2 and 3.3 are drawn. With the increasing values of solid volume

fraction ψ, both temperature and velocity fields increase. Moreover, the larger value of ψ, boosted the momentum and thermal boundary layer thickness. As amalgamation of nano-particles in fluid leads to higher thermal conductivity thus fluid's temperature increases. Figures $3.4 - 3.6$ depict the influence of the radius of curvature parameter k_c on temperature, velocity and concentration profiles. Rising values of k_c consequently increase the temperature field and fluid velocity while concentration profile reduces. As a result of increase in the radius, the curvature parameter is increased consequently flow enhances by offering more resistance, therefore temperature increases.

Velocity field variations for several estimates of magnetic parameter M are exhibited in Figure 3.7. Here the growing values of M are reason of decrease in the magnitude of fluid velocity. This occurs due to the resistive force *i.e.,* Lorentz force, originated by the magnetic field lowering the velocity of the fluid's flow. Figures 3.8 and 3.9 illustrate the characteristics of Biot number Bi, heat generation and absorption parameter λ^* on temperature field, respectively. Figure 3.8 shows that for higher estimates of Biot number Bi , convective heat transfer coefficient enhances leading towards the maximum surface temperature which appreciably enhance the temperature distribution and the thickness of the thermal boundary layer . The behavior of λ^* as illustrated in Figure 3.9 verses the temperature distribution, and the thickness of boundary layer increasing for growing values of heat absorption/ generation parameter λ^*.

Figures 3.10 and 3.11 explain the effect on temperature distribution by nonlinear radiation parameter Ra and Prandtl number Pr. It is noticed that with the increasing Prandtl number Pr, temperature field falls as Prandtl number has reciprocal relationship with the thermal diffusivity. Therefore, quick rise in the Prandtl number Pr, lowers temperature and thermal boundary layer thickness. The enhancement in nonlinear radiation parameter Ra increases temperature profile. Physically, the radiative heat flux increases q_r against the rising values of Ra, which eventually boosts the temperature of the fluid. Figure 3.12 illustrates the impression on concentration distribution by the Schmidt number Sc. Increasing values of Sc, produce a decline in concentration field. Since, the

Schmidt number is conversely related to the Brownian diffusion coefficient. This is the reason that a rise in the Sc, produce a decay in diffusion coefficient which brings about a reduction in concentration and its associated boundary layer thickness.

The impact on Entropy generation by the Brinkman number's (Br) is explained in Figure 3.13. It is obvious from the illustration that entropy optimization is enhanced for rising values of Br. The reason behind this is that extra heat is produced between layers of the fluid due to increased values of Br. Figure 3.14 depicts the relationship of the magnetic parameter M and entropy generation. Similar characteristic as described in case of Br is observed here. The higher values of M indicate that Lorentz force is stronger which eventually strengthen the dissipation energy and this is major reason of irreversibility.

Table 3.3 illustrated that the influence on Skin friction coefficient $-\frac{1}{2}\,\mathrm{Re}_x^{0.5}\,C_{fx}$ by k_c, ψ and M. The decrease in the surface drag force coefficient is observed along with the rising values of radius of curvature parameter k_c. Foregoing illustrates that enhancement in k_c reduces the radius of curvature of the surface consequently offers a less resistance to the fluid particles and ultimately decay the surface drag force. An opposing tendency is experimented in case of M and ψ. It is identified that the skin friction profile is directly proportional to magnetic parameter M and solid volume fraction ψ.

Table 3.4 shows that the impact on Nusselt number $-\left(\mathrm{Re}_x\right)^{-0.5}\,Nu_x$ due to variation in the Biot number Bi, nonlinear radiation parameter Ra, radius of curvature parameter k_c and nanoparticle volume fraction ψ. It is observed that the surface heat transfer rate upsurges for elevated value of Bi, k_c , ψ and Ra.

Table 3.5 describes specific upshot of Sherwood number $\left(\mathrm{Re}_x\right)^{-0.5}\,Sh_x$ for verious values of curvature parameter k_c,magnetic parameter M and the Schmidt number Sc. It is apparent that the Sherwood number $\left(\mathrm{Re}_x\right)^{-0.5}\,Sh_x$ enhances owing to growing values of Sc. Though, it is retreating for rising value of k_c and$M$.

Table 3.2 : Results' comparison, for Skin friction coefficient $\frac{1}{2}(\mathrm{Re}_x)^{\frac{1}{2}}C_{fx}$ when $m = 1$ and $\psi = 0.0$

k_c	Present result	Sanni et al. [26]
1000	1.00079	1.0008
100	1.00690	1.0070
50	1.01400	1.0140
20	1.03540	1.0355
10	1.07341	1.0734
5	1.15760	1.1576

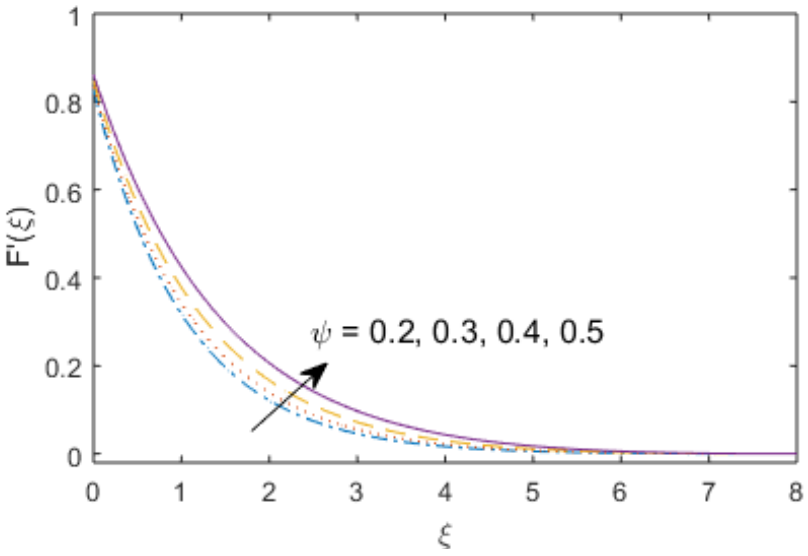

Figure 3.2 : Velocity distribution $F'(\xi)$ influenced by ψ

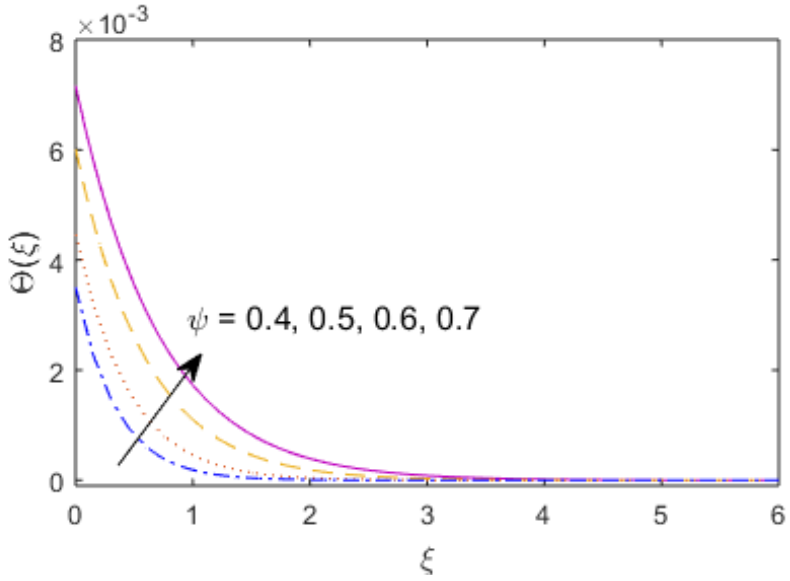

Figure 3.3 : Temperature profile $\Theta(\xi)$ influenced by ψ

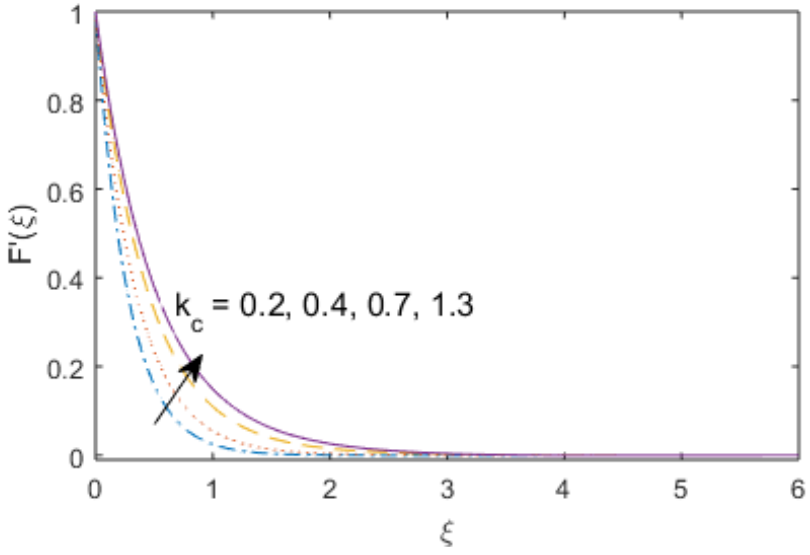

Figure 3.4 : Velocity distribution $F'(\xi)$ influenced by k_c

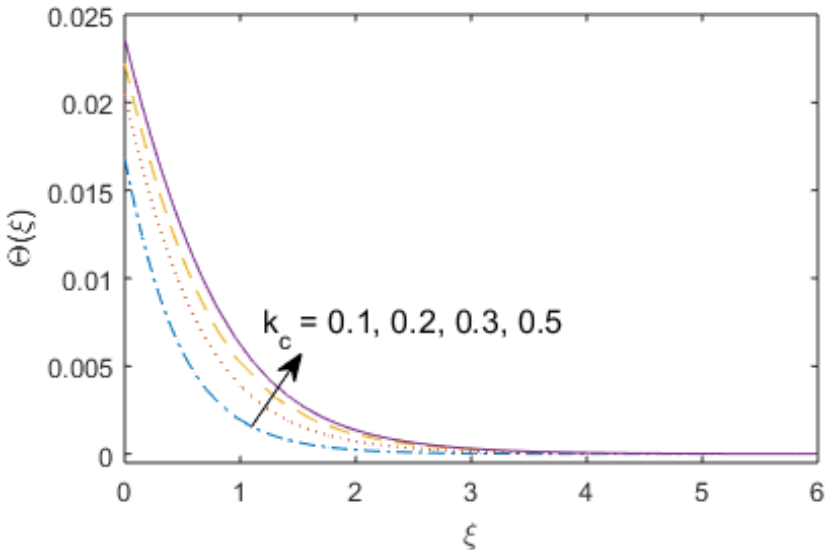

Figure 3.5 : Temperature profile $\Theta(\xi)$ influenced by k_c

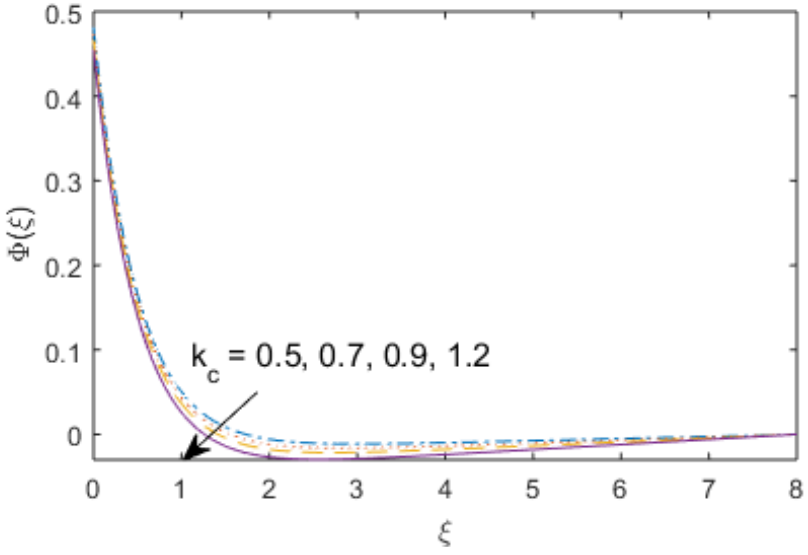

Figure 3.6 : Concentration profile $\Phi(\xi)$ influenced by k_c

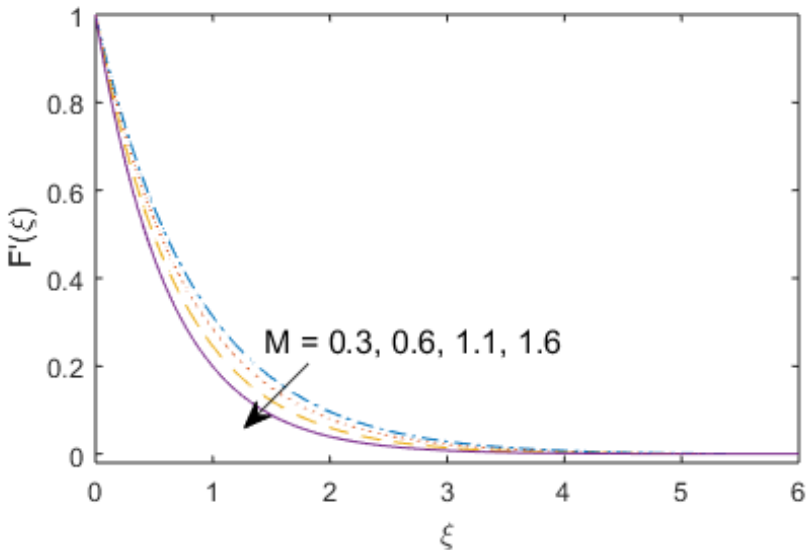

Figure 3.7 : Velocity profile $F'(\xi)$ influenced by M

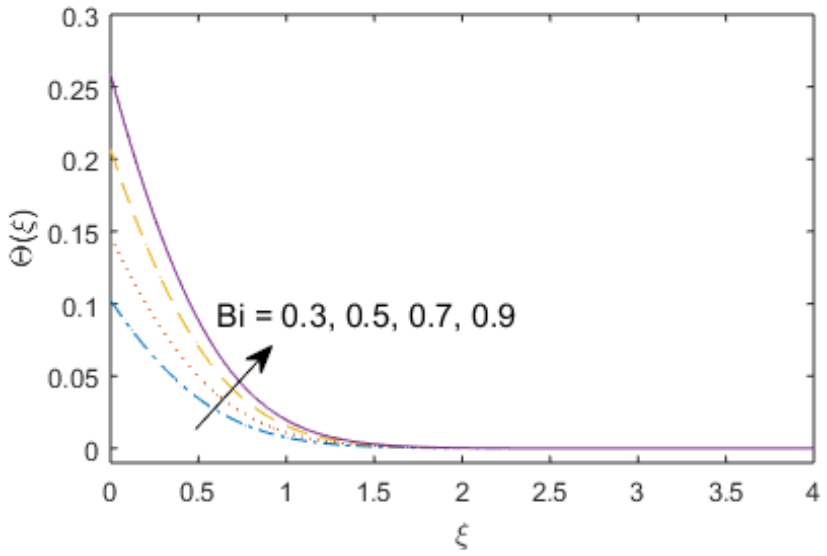

Figure 3.8 : Temperature distribution $\Theta(\xi)$ influenced by Bi

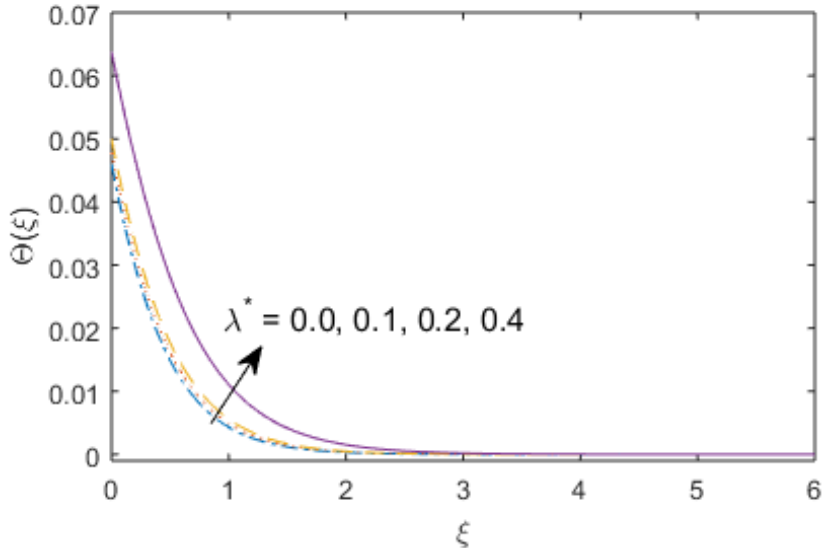

Figure 3.9 : Temperature distribution $\Theta(\xi)$ influenced by λ^*

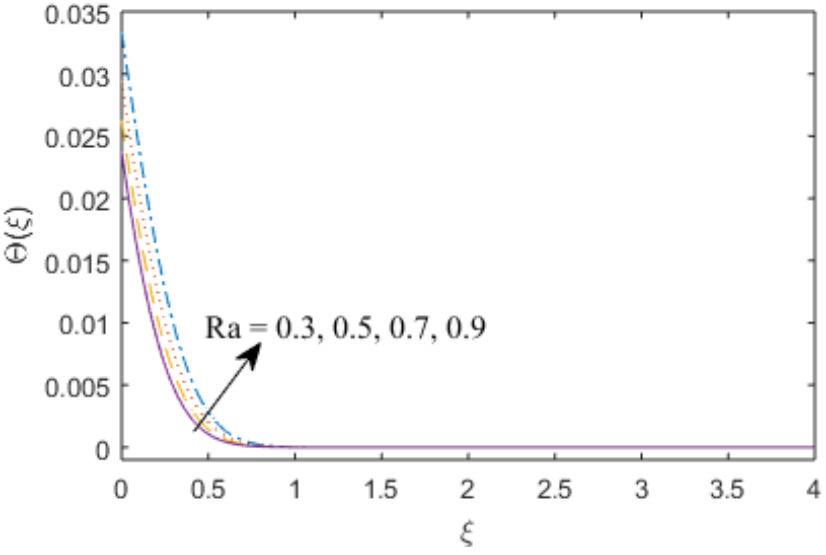

Figure 3.10 : Temperature distribution $\Theta(\xi)$ influenced by Ra

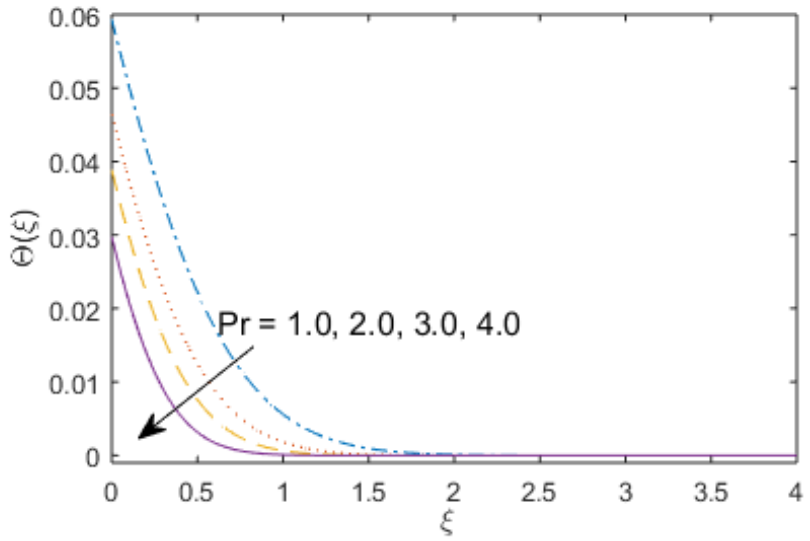

Figure 3.11 : Temperature distribution $\Theta(\xi)$ influenced by Pr

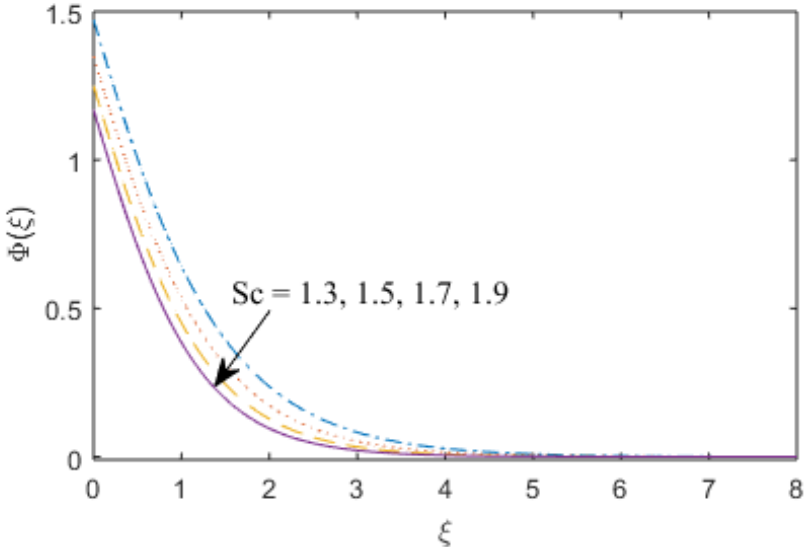

Figure 3.12 : Concentration profile $\Phi(\xi)$ influenced by Sc

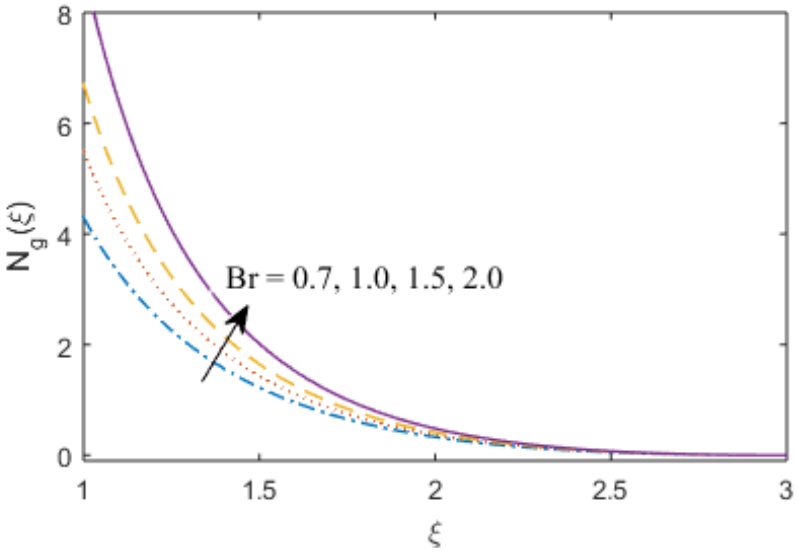

Figure 3.13: Entropy generation $N_g(\xi)$ influenced by Br

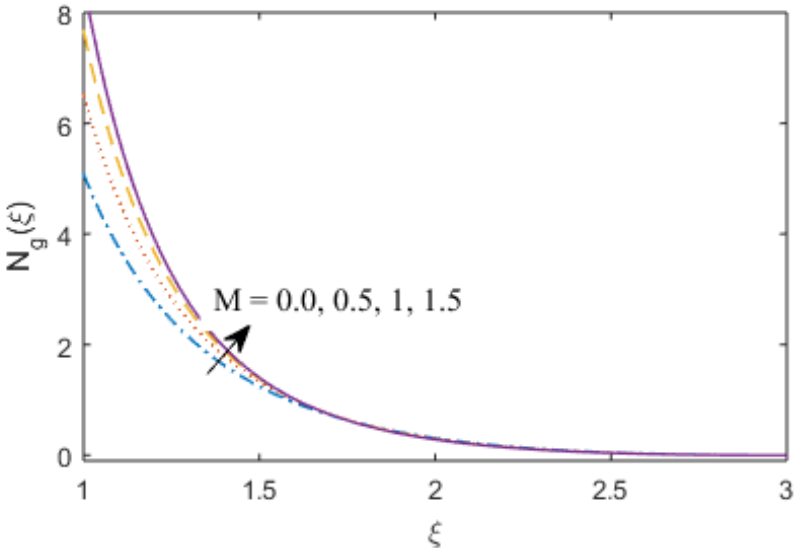

Figure 3.14: Entropy generation $N_g(\xi)$ influenced by M

Table 3.3**:** Numerical value of $-1/2(\mathrm{R}e_x)^{0.5}C_f$ via various significant parameters with fixed value of $\lambda^* = \Theta_W = Sc = 0.5, Ra = Bi = 0.1$ and $\mathrm{Pr} = 10$

k_c	M	ψ	$-1/2(\mathrm{R}e_x)^{0.5}C_f$
0.8	0.1	0.1	1.6266860
1			1.3013488
1.3			1.0010376
1.9			0.68492044
10	0.1		0.13013488
	0.2		0.13013674
	0.3		0.13013916
	0.4		0.13014128
	0.1	0.2	0.17469281
		0.3	0.24392421
		0.4	0.35860957
		0.5	0.56568542

Table 3.4**:** Numerical value of $(\mathrm{Re}_x)^{-0.5}Nu_x$ via various significant parameters with fixed value of $M = 0.1, \Theta_W = \lambda^* = Sc = 0.5$ and $\mathrm{Pr} = 10$

Bi	ψ	k_c	Ra	$-(\mathrm{Re}_x)^{-0.5}Nu_x$
0.1	0.1	10	0.1	0.87237079
0.2				0.87825809
0.3				0.88508781
0.4				0.89303016
0.1	0			0.97053572
	0.05			0.92374204
	0.1			0.89303016
	0.15			0.83662429
	0.1	0.2		0.89301040
		0.3		0.89301720
		0.4		0.89302125
		0.5		0.89302367
		10	0	0.87471389
			0.1	0.88383935
			0.2	0.89303016
			0.3	0.90229133

Table 3.5**:** Numerical value of $(\mathrm{Re}_x)^{-0.5} Sh_x$ via various significant parameters with fixed value of $\lambda^* = \Theta_W = 0.5, \psi = Ra = Bi = 0.1$ and $\mathrm{Pr} = 10$

Sc	k_c	M	$(\mathrm{Re}_x)^{-0.5} Sh_x$
0.5	10	0.1	0.38325
1			0.59354
2			0.92268
5	5	0.1	1.60150
	10		1.58090
	50		1.56230
5	10	0.3	1.56270
		0.5	1.54600
		0.7	1.53040

Chapter 4

Radiative hybrid nanofluid flow with stratification and slip over a curved surface

4.1 Mathematical modeling

We consider time dependent (2D) and incompressible boundary layer flow of hybrid nanofluid past a curved surface. In the existence of nonlinear heat-flux and heat generation/absorption, flow analysis is adopted with themal stratification. A curvilinear coordinate system is adopted in such a manner that x-axis is directed along the curved stretching surface while the r-axis normal to it. Here, $U_W = Sx$, (S is the positive real number), is the stretching velocity vary linearly with distance from the origin and $\overline{R}$ is the radius of the curved surface.In the r-direction, an invariable magnetic field is applied. Assuming the magnetic Reynold number to be very small, the effect of induced and electric magnetic field can be ignored.

$$((r + \overline{R})V))_r + \overline{R}Ux = 0, \tag{4.1}$$

$$p_r = \frac{\rho_{nf}}{r+\overline{R}}U^2, \tag{4.2}$$

$$VU_r + \frac{\overline{R}}{r+\overline{R}}UU_x + \frac{1}{r+\overline{R}}UV = -\frac{\overline{R}}{(r+\overline{R})\rho_{nf}}p_x + \frac{\mu_{nf}}{\rho_{nf}}(U_{rr} + \frac{1}{r+\overline{R}}U_r,$$

$$-\frac{1}{(r+\overline{R})^2}U) - \sigma^*\frac{\beta_0^2}{\rho_{nf}}U, \tag{4.3}$$

$$VT_r + \frac{\overline{R}}{(r+\overline{R})}T_x = \alpha(T_{rr} + \frac{1}{r+\overline{R}}T_r - \frac{Q^*}{(\rho C_{p)_{nf}}}(T_\infty - T)$$

$$+\frac{1}{(r+\overline{R})(\rho C_p)_{nf}}((r+\overline{R})q_r)_r. \tag{4.4}$$

The following suitable boundary condition are in the form:

$$V = 0, U = U_W(x) + L(U_r - \frac{1}{r+\overline{R}}U),$$

$$T = T_W = T_0 + n_1 x, \text{ at } \mathrm{r} = 0,$$

$$U \to 0,\ U_r \to 0,\ T = T_\infty = T_0 + n_2 x \text{ as } r \to \infty. \tag{4.5}$$

The Thermo physical traits of the hybrid nano-liquid are mentioned in Table 4.1.

Table 4.1 : Ethylene glycol($C_2H_6O_2$) and Nickel-zinc ferrite ($NiZnFe_2O_4$) having the values of ρ (density), k (thermal conductivity) and C_p (heat capacity) [47-52] .

Thermo physical properties	Ethylene glycol	Nickel-zinc ferrite
$C_p(Jkg^{-1}\ k^{-1})$	2382.0	710.0
k $(Wm^{-1}K^{-1})$	0.2490	6.3
ρ (kgm^{-3})	1116.6	4800.0
Pr	204.0	–

Thermo mechanical properties represented in the mathematical form as:

$$\mu_{nf} = \mu_f(1-\psi)^{-2.5},\ \alpha = \frac{k_{nf}}{(\rho C_p)_{nf}},$$

$$\frac{\rho_{nf}}{\rho_f} = (1-\psi) + \psi\frac{\rho_s}{\rho_f},\ \frac{(\rho C_p)_{nf}}{(\rho C_p)_f} = (1-\psi) + \psi\frac{(\rho C_p)_s}{(\rho C_p)_f},$$

$$\frac{k_{nf}}{k_f} = \frac{2\psi(k_f - k_s) + (2k_f + k_s)}{\psi(k_f - k_s) - (2k_f - k_s)}. \tag{4.6}$$

Nonlinear radiation heat-flux (under Rosseland's approximation) used in equation (4.4), is given by:

$$q_r = \frac{4\overline{\sigma}}{3\overline{K}}(T^4)_r = \frac{16\overline{\sigma}}{3\overline{K}}T^3T_r. \tag{4.7}$$

The corresponding nonlinear ordinary differential equation of above mathematical model are obtained by utilizing subsequent transformation.

$$\xi = (\frac{S}{\upsilon_f})^{\frac{1}{2}}r,\quad p = \rho_f S^2x^2P(\xi),\ T = T_\infty(1 + (\frac{1}{\Theta_W + S_t})\Theta),$$

$$\Theta = \frac{T - T_\infty}{T_W - T_0},\ U = SxF'(\xi),\ V = \frac{-\overline{R}}{r + \overline{R}}(S\upsilon_f)^{\frac{1}{2}}F(\xi). \tag{4.8}$$

Here,the superscript ($'$) indicates the derivative w.r.t ξ , and substituting temperature ratio parameter $\Theta_W = \frac{T_0}{T_W - T_0}$ .the above tranformation (4.8) satisfaction of equation (4.1) is inevitable. However, equations $(4.2) - (4.4)$ reduce

$$P' = (1 - \psi + \psi\frac{\rho_s}{\rho_f})\frac{F'}{\xi - k_c} \tag{4.9}$$

$$\frac{2k_c}{\xi + k_c}P = (1 - \psi + \psi\frac{\rho_s}{\rho_f})(\frac{k_c}{(\xi + k_c)^2}FF' + \frac{k_c}{\xi + k_c}(FF'' - F'^2) - MF')$$
$$+ (1-\psi)^{-2.5}(F''' + \frac{1}{(\xi + k_c)}F'' - \frac{1}{(\xi + k_c)^2}F''') \tag{4.10}$$

$$\frac{1}{\Pr}(\frac{k_{nf}}{k_f}+R_a(1+(\frac{1}{\Theta_W+S_t})\Theta)^3)(\Theta''+\frac{1}{\xi+k_c}\Theta')+\lambda^*\Theta$$

$$+(1-\psi+\psi\frac{(\rho C_p)_s}{(\rho C_p)_f})\frac{k_c}{\xi+k_c}\left(F\Theta'-F'\Theta-S_tF'\right)$$

$$+\frac{3R_a}{\Pr}(1+(\frac{1}{\Theta_W+S_t})\Theta)^2(\frac{1}{\Theta_W+S_t})\Theta'^2=0, \tag{4.11}$$

$$F(0)=0,\ F'(0)=1+\kappa\left(F''-\frac{F'}{k_c}\right),\ \Theta(0)=(1-S_t)$$

$$F'(\infty)\to 0,\ F''(\infty)\to 0,\ \Theta(\infty)\to 0. \tag{4.12}$$

Eliminating the pressure term $P(\xi)$ by solving equations (4.9) and (4.10), resulting in the following equation:

$$F^{iv}+\frac{2}{\xi+k_c}F'''-\frac{1}{(\xi+k_c)^2}F''+\frac{1}{(\xi+k_c)^3}F'+(1-\psi)^{2.5}\left(1-\psi+\psi\frac{\rho_s}{\rho_f}\right)\{\frac{k_c}{\xi+k_c}(FF'''+F'F'')$$

$$-\frac{k_c}{(\xi+k_c)^2}\left(F'^2-FF''\right)-\frac{k_c}{(\xi+k_c)^3}FF'\}-(1-\psi)^{2.5}M\left(\frac{1}{\xi+k_c}F'+F''\right)=0. \tag{4.13}$$

with

$$k_c=\overline{R}\left(\frac{S}{\upsilon_f}\right)^{\frac{1}{2}},\ S_t=\frac{n_1}{n_2},\ \kappa=L\left(\frac{S}{\upsilon_f}\right)^{\frac{1}{2}},\ M=\sigma^*\frac{\beta_0^2}{\rho_f S}$$

$$\Pr=\frac{\upsilon_f}{\alpha^*},\ \lambda^*=\frac{Q^*}{S(\rho C_p)_f},\ R_a=\frac{16\overline{\sigma}}{3k_f\overline{k}}T_\infty^3. \tag{4.14}$$

Mathematical expression of surface drag force coefficient (C_{fx}) and Nusselt number (Nu_x) are appended as follows:

$$C_{fx}=\frac{2\tau_{rx}}{\rho_f U_W^2},\ Nu_x=\frac{xq_{_W}}{k_f(T_W-T_\infty)} \tag{4.15}$$

where shear stress and heat flux of wall given as:

$$\tau_{rx}=\mu_{nf}\left(U_r-\frac{1}{r+\overline{R}}U\right)_{r=0},\ q_{_W}=-\left((q_r)+T_r\right)_{r=0} \tag{4.16}$$

The transformations (4.8) and (4.16) formulate equation (4.15) as:

$$\frac{1}{2}\left(\mathrm{R}e_x\right)^{\frac{1}{2}} C_{fx} = (1-\psi)^{-2.5}\left(F''(0) + \frac{F'(0)}{k_c}\right), \tag{4.17}$$

$$\left(\mathrm{R}e_x\right)^{-\frac{1}{2}} Nu_x = -\left[Ra\left(1 + (\frac{1}{\Theta_W + S_t})\Theta(0)\right)^3 + \frac{k_{nf}}{k_f}\right]\Theta'(0). \tag{4.18}$$

Reynolds numbers is given as:

$$\mathrm{R}e_x = \frac{U_W}{\upsilon_f}x.$$

4.2 Results and discussions

This part is devoted for visualizing the influenced velocity and temperature profile illustrated in Figures $4.1 - 4.10$, versus Hartmann number, slip parameter, heat generation/absorption parameter, radiation parameter, themal stratification parameter, solid volume fraction and Prandtl number. The nonlinear differential equations are numerically evaluated for the problem's better understanding. The non-linear ordinary differential equations (4.12) and (4.14) collectively are solved numerically by adopting the MATLAB's function *bvp4c* and using given boundary conditions in equation (4.13). This adopted procedure at first involves the system of equations (4.12), (4.14) to be reduced to first order equations incorporated with the boundary conditions. Suitable initial guesses fulfilling the boundary conditions are subsequently decided on. The values of other parameters are fixed as $M = \psi = \Theta_W = S_t = 0.1$, $\lambda^* = Ra = 0.5$, $\mathrm{Pr} = k_c = 10$ and $\kappa = 0.2$.

The variations in the velocity distributions $F'(\xi)$ and temperature profiles $\Theta(\xi)$ are illustrated in Figures 4.1 and 4.2, concerning various estimates of radius of curvature k_c. The amplification of fluid velocity due to larger values of k_c , means that the boundary layer thickness of velocity profile raises with radius of curvature k_c. It is because of the causal relation between the radius and curvature parameters. Rise in the value of radius curvature k_c causes rise in temperatures distribution $\Theta(\xi)$. Physically it means that the

flow enhances by offering more resistance, therefore temperature increases. Observing the impression of solid volume fraction on velocity and temperature distributions, Figures 4.3 and 4.4 are drawn. With the increasing values of solid volume fraction ψ, both velocity and temperature fields increase. Moreover, the larger value of ψ, boost the momentum and thermal boundary layer thickness. As amalgamation of nanoparticles in fluid leads to higher thermal conductivity thus increasing fluid temperature.

Velocity field variations for several estimates of M are exhibited in Figure 4.5. Here, the increasing values of M are reason of decrease in the magnitude of fluid velocity. This occurs due to the resistive force *i.e.,* Lorentz force, originated by the magnetic field lowering the velocity of the fluid's flow. As observed in Figure 4.6, with mounting the estimates of κ, drop off the velocity of the liquid. Rise in slip parameter κ decreases the thickness of velocity boundary layer. The increase in velocity slip parameter κ produces decrease in the thickness of velocity boundary layer. Velocity slip parameter κ with physical increase causes small deformation in the fluid due to weak adhesive forces. Figure 4.7 exhibits the Influence of the slip parameter κ on the temperature distribution. Growing the values of the κ causes an enhancement in temperature and temperature boundary layer of nanoparticles caused by the transportation of nanoparticles.

Figure 4.8 displays the hybrid nanofluid temperature distribution with numerous estimates of thermal stratification parameter S_t. The reduction is noted in temperature distribution due to S_t higher estimates. It is observed that in absence of thermal stratification *i.e.,* $(S_t = 0)$, prescribed surface temperature is attained. Higher amount of stratification lowers the variation between the ambient temperature and surface temperature, thus it causes of thinning in the fluid of the thermal boundary layer by lowering fluid temperature. The behavior of heat absorption/generation parameter λ^* is portrayed in Figure 4.9, the thermal boundary layer thickness and temperature profile increase for growing estimate values of heat absorption/generation parameter.

Figures 4.10 and 4.11 explain the effect on temperature distribution by nonlinear radiation parameter Ra and Prandtl number Pr. The results show that rise in Pr reduces

temperature field. As Prandtl number have reciprocal association with the thermal diffusivity. Therefore quick rise in the Pr lowers temperature and thermal boundary layer thickness. The enhancement in nonlinear radiation parameter Ra increases temperature profile. Physically, the radiative heat flux q_r increases against the rising values of Ra eventually boosts the temperature of the fluid.

Table 4.2 depicts the outcome of numerous parameters on -$\frac{1}{2}$ $(\mathrm{R}e_x)^{\frac{1}{2}}$ C_{fx} and -$(\mathrm{R}e_x)^{-\frac{1}{2}}$ Nu_x. This is established that for greater estimates of magnetic parameter M and ψ drag force coefficient grows, however it declines owing to higher estimates of slip and curvature parameters. The considerable enhancement in Skin friction coefficient is caused by the increase in ψ. Physically, the amalgamation of nanoparticles within the fluid and on the surface, upsurges the surface friction. The reduction in drag force coefficient is detected as value of radius of curvature increases, it illustrates that rise in reduces curvature of the surface. Consequently, reducing resistance to the fluid particles which decline the -$\frac{1}{2}$ $(\mathrm{R}e_x)^{\frac{1}{2}}$ C_{fx}.

As viewed in the Table, the estimated values of Nusselt number -$(\mathrm{R}e_x)^{-\frac{1}{2}}$ Nu_x are raised for higher estimates of solid volume fraction ψ , slip, radius of curvature and radiation parameters and it is on decline by rising values of magnetic, thermal stratification and heat generation. It is observed that rise in the value of Ra raises the magnitude of rate of heat flux which eventually increases the heat transfer rate. It is noticed that escalating value of radius of curvature causes decrease in the magnitude of local Nussselt number, since the decrease in radius of curvature cause increase in fluid temperature. The rising values of stratification cause decrease in heat flux rate. It is noticed that due to decline in temperature variation between fluid of ambient and surface of the curve, the values of Nusselt number decrease.

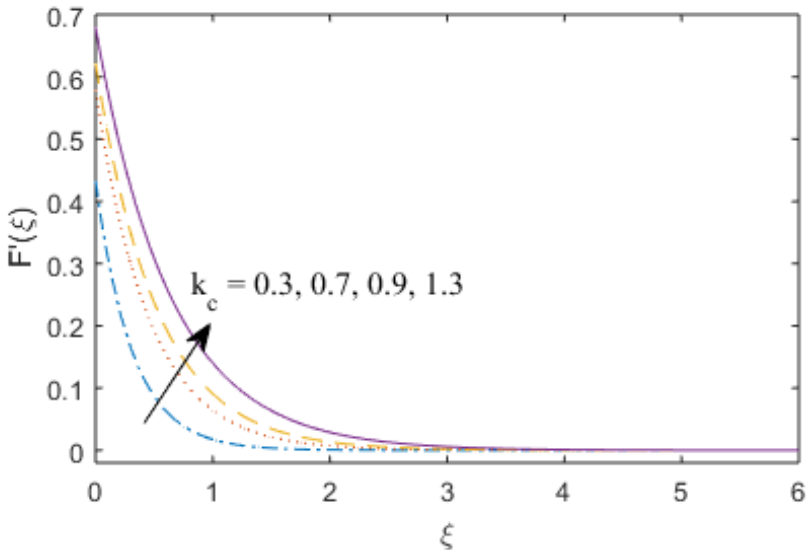

Figure 4.1 : Velocity profile $F'(\xi)$ influenced by k_c

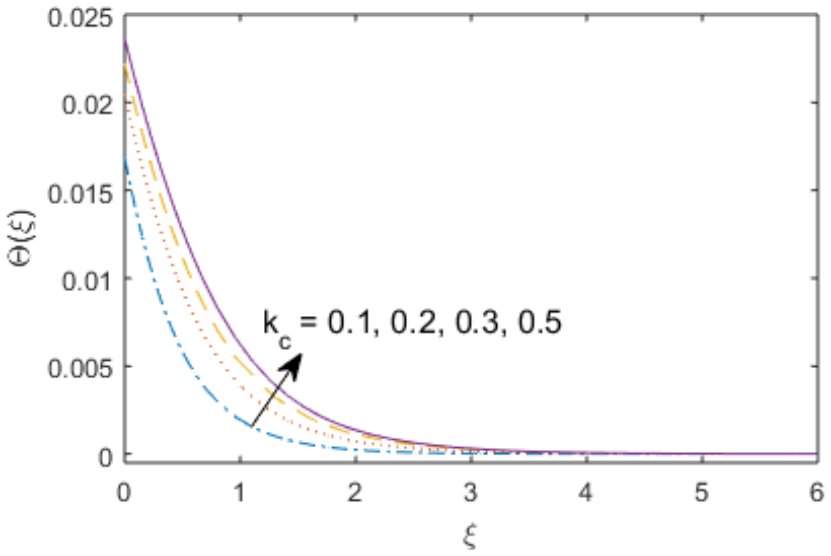

Figure 4.2 : Temperature profile $\Theta(\xi)$ influenced by k_c

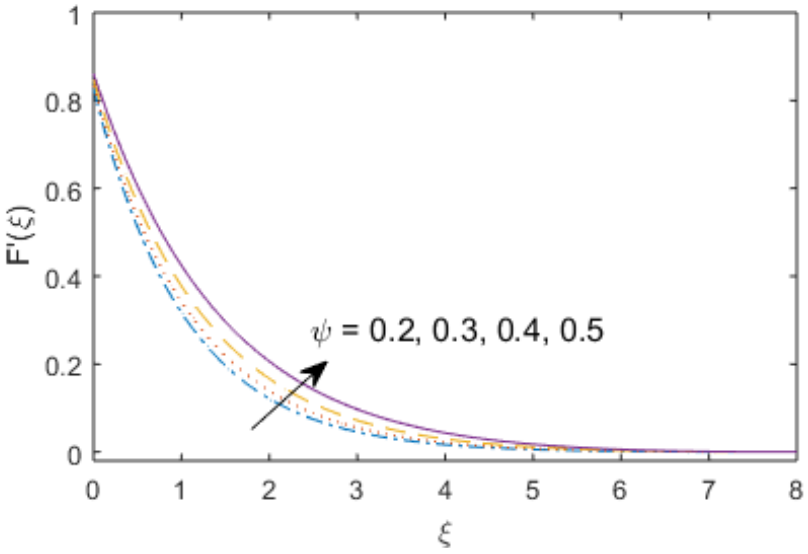

Figure 4.3 : Velocity profile $F'(\xi)$ influenced by ψ

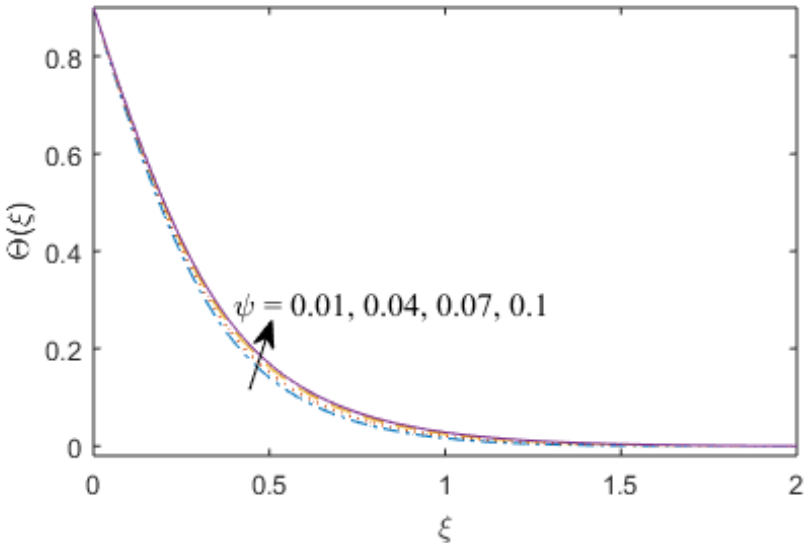

Figure 4.4 : Temperature profile $\Theta(\xi)$ influenced by ψ

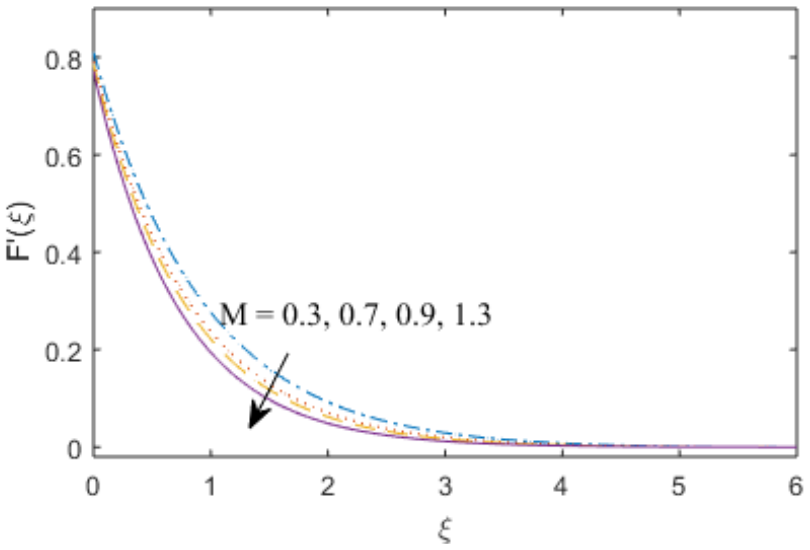

Figure 4.5 : Velocity profile $F'(\xi)$ influenced by M

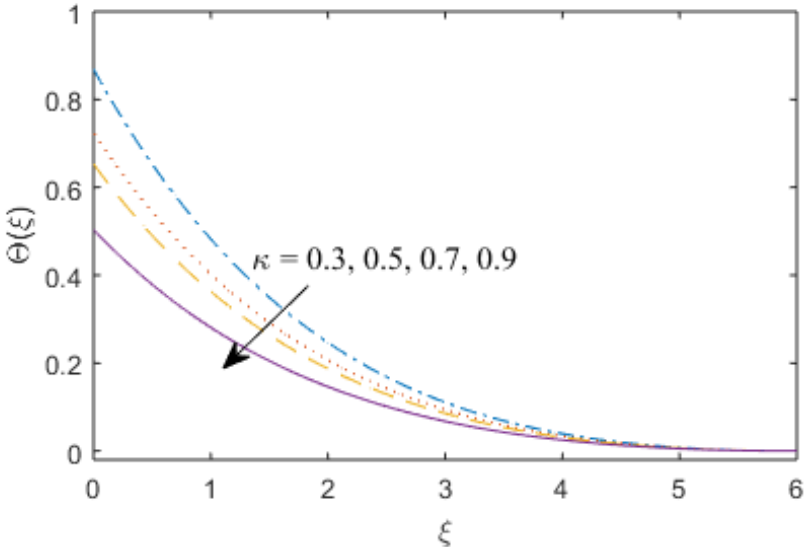

Figure 4.6 : Velocity profile $F'(\xi)$ influenced by κ

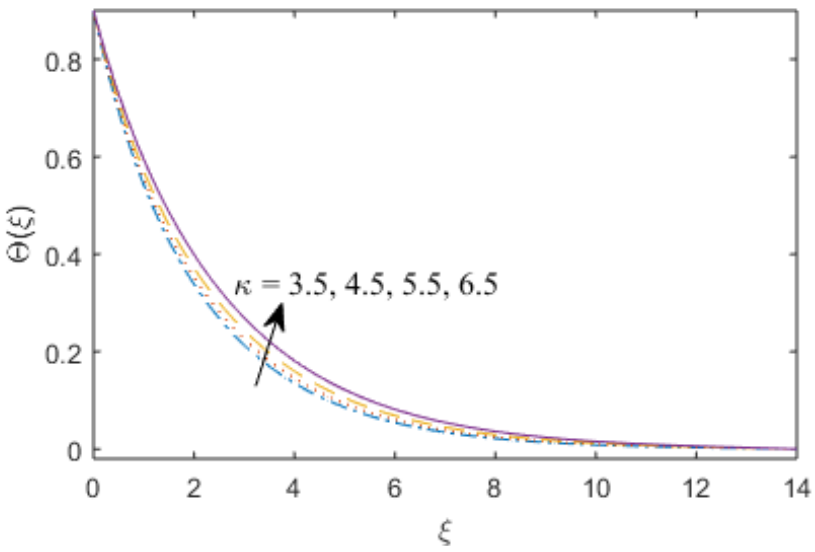

Figure 4.7 : Temperature profile $\Theta(\xi)$ influenced by κ

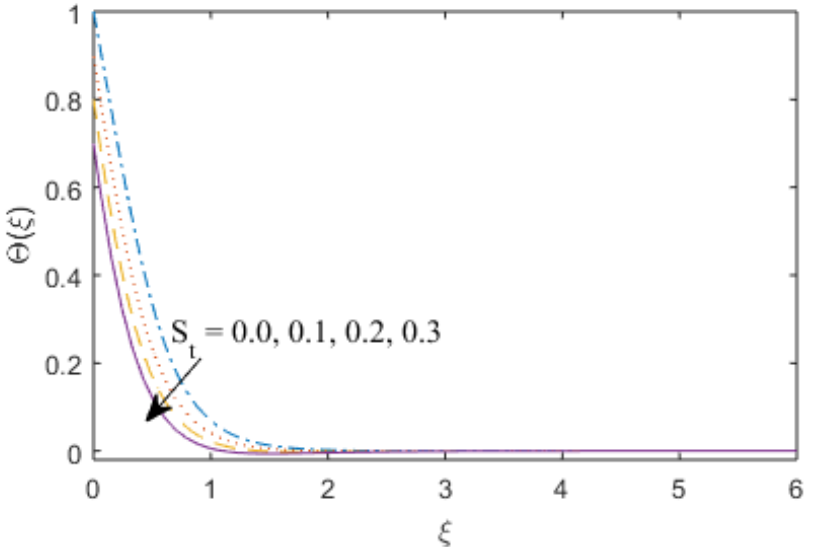

Figure 4.8 : Temperature profile $\Theta(\xi)$ influenced by S_t

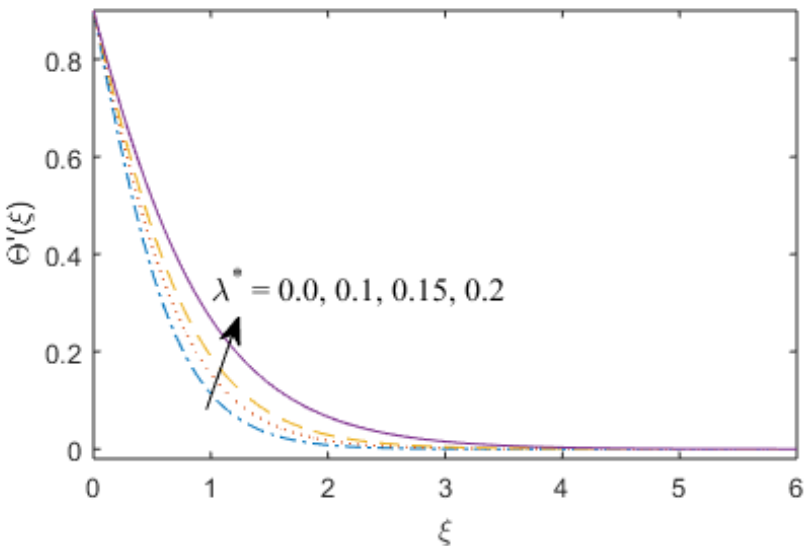

Figure 4.9 : Temperature profile $\Theta(\xi)$ influenced by λ^*

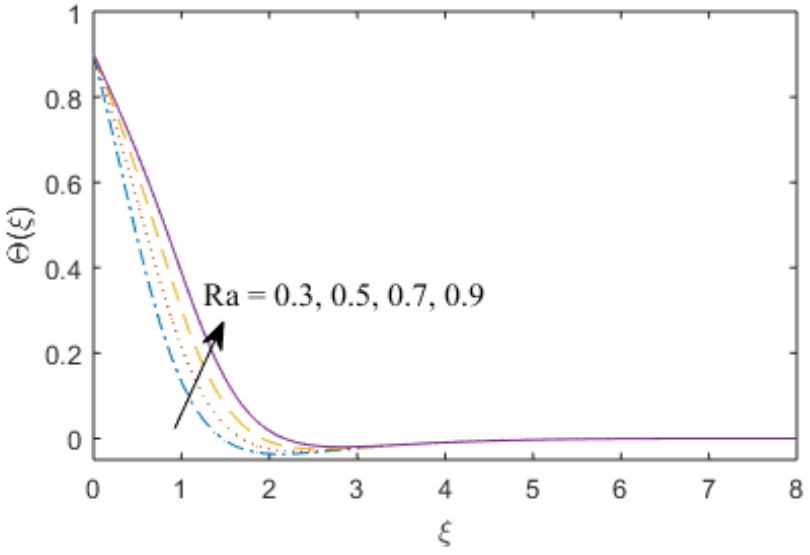

Figure 4.10 : Temperature profile $\Theta(\xi)$ influenced by Ra

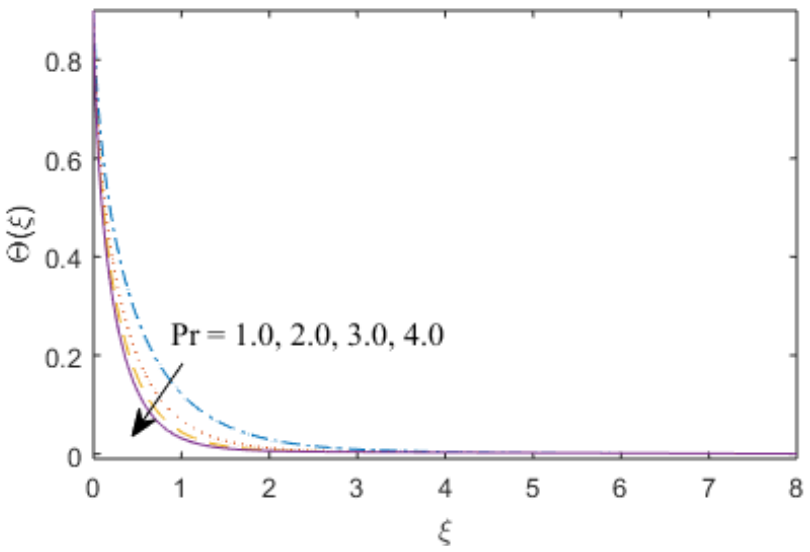

Figure 4.11 : Temperature profile $\Theta(\xi)$ influenced by Pr

Table 4.1 : Numerical outcomes of the $-\frac{1}{2}\left(\mathrm{Re}_x\right)^{\frac{1}{2}} C_{fx}$ and $\left(\mathrm{Re}_x\right)^{-\frac{1}{2}} Nu_x$.

κ	S_t	λ^*	Ra	M	ψ	k_c	$-\frac{1}{2}\left(\mathrm{Re}_x\right)^{\frac{1}{2}} C_{fx}$	$-\left(\mathrm{Re}_x\right)^{-\frac{1}{2}} Nu_x$
0.1	0.1	0.5	0.5	0.1	0.1	10	1.3291553	3.7670128
0.2							1.1728782	4.2556719
0.3							1.0526318	4.7740485
0.1	0.2						1.3291553	4.6840764
	0.3						1.3291553	4.6405272
	0.4						1.3291553	4.6350093
	0.1	0.1					1.3291553	6.6834651
		0.2					1.3291553	6.2755559
		0.3					1.3291553	5.8318231
		0.5	0.2				1.3291553	4.1672184
			0.3				1.3291553	4.3855480
			0.4				1.3291553	4.5881019
			0.5	0.2			1.3668642	4.7011298
				0.3			1.4032186	4.6266452
				0.4			1.4383243	4.5498593
				0.1	0.2		1.7288174	5.0628829
					0.3		2.2802923	5.6515857
					0.4		3.0923874	6.3707609
					0.1	1	2.8818797	3.7962643
						2	2.0129193	5.0363786
						3	1.7076896	9.4400293

Chapter 5

Conclusions and future work

In this thesis two problems have been analysed where first problem is review paper and second problem is the extension work. Conclusion of both of the problems are as follows:

5.1 Conclusions (Chapter 3)

- The mounting velocity, rising temperature field and fading concentration distribution are due to the reason of effective amplification of curvature parameter.
- An increased axial velocity field is generated due to major influence of magnetic parameter.
- The rising behavior of temperature and velocity profiles is because of increasing estimates of the solid volume fraction.
- There is an improvement in the temperature profile with rising values of Biot number and heat generation/absorption parameter.
- The larger values of magnetic parameter M and solid volume fraction ψ cause the increase in values of fraction factor profile but it drop off for radius of curvature parameter k_c

- The growing values of radius of curvature parameter k_c and nonlinear radiation parameter Ra increase the Nusselt number $-(\mathrm{R}e_x)^{-0.5} Nu_x$.

5.2 Conclusions (Chapter 4)

- Velocity and temperature distributions have increasing behaviors from the curve when curvature parameter is increased.
- The velocity profile decreases due to increment in the magnetic and slip parameters.
- The temperature distribution upsurges with inflated thermal radiation and slip parameters but reduces for growing values of stratification parameter.
- The values of Skin friction coefficient enhance by growing magnetic parameter's values and a decline is observed when slip parameter and radius of curvature parameter have higher values.
- The Nusselt number grows higher owing to raised values of radiation parameter, slip parameter and radius of curvature parameter, while a reversed behavior is noticed for growing values of thermal stratification.

5.3 Future work

The current study can be extended to the subsequent models as well:

- The model may be extended to homogenous and heterogeneous reactions.
- The momentum equation may be improved by adding the effects of Darcy-Forchheimer and buoyancy effects.
- The energy equation can be enhanced by adding the Cattaneo-Christov heat flux.
- The boundary condition may be exchanged with melting heat and mass transfer.

Bibliography

[1] Maxwell, J. C. (1873). A treatise on electricity and magnetism (Vol. 1). Oxford: Clarendon Press.

[2] Choi, S. U. S., Singer, D. A., & Wang, H. P. (1995). Developments and applications of non-Newtonian flows. Asme Fed, 66, 99-105.

[3] Masuda, H., Ebata, A., Teramae, K., Hishinuma, N., & Ebata, Y. (1993). Alteration of thermal conductivity and viscosity of liquid by dispersing ultra-fine particles (dispersion of γ-Al2O3, SiO2 and TiO2 ultra-fine particles). Netsu Bussei, 7(4), 227–233.

[4] Lee, S., Choi, S. S., Li, S. A., & Eastman, J. A. (1999). Measuring thermal conductivity of fluids containing oxide nanoparticles. Journal of Heat transfer, 121(2), 280-289.

[5] Pastoriza-Gallego, M. J., Lugo, L., Legido, J. L., & Piñeiro, M. M. (2011). Rheological non-Newtonian behaviour of ethylene glycol-based Fe_2O_3 nanofluids. Nanoscale research letters, 6(1), 560.

[6] Hayat, T., & Nadeem, S. (2017). Heat transfer enhancement with Ag–CuO/water hybrid nanofluid. Results in Physics, 7, 2317-2324.

[7] Nadeem, S., Abbas, N., & Khan, A. U. (2018). Characteristics of three dimensional stagnation point flow of Hybrid nanofluid past a circular cylinder. Results in Physics, 8, 829-835.

[8] Morrison, S. A., Cahill, C. L., Carpenter, E. E., Calvin, S., Swaminathan, R., McHenry, M. E., & Harris, V. G. (2004). Magnetic and structural properties of nickel zinc ferrite nanoparticles synthesized at room temperature. Journal of Applied Physics, 95(11), 6392-6395.

[9] Naughton, B. T., & Clarke, D. R. (2007). Lattice expansion and saturation magnetization of nickel–zinc ferrite nanoparticles prepared by aqueous precipitation. Journal of the American Ceramic Society, 90(11), 3541-3546.

[10] Virden, A. E., & O'Grady, K. (2005). Structure and magnetic properties of NiZn ferrite nanoparticles. Journal of Magnetism and Magnetic Materials, 290, 868-870.

[11] Shahane, G. S., Kumar, A., Arora, M., Pant, R. P., & Lal, K. (2010). Synthesis and characterization of Ni–Zn ferrite nanoparticles. Journal of Magnetism and Magnetic Materials, 322(8), 1015-1019.

[12] Sheikholeslami, M., Ganji, D. D., & Rashidi, M. M. (2015). Ferrofluid flow and heat transfer in a semi annulus enclosure in the presence of magnetic source considering thermal radiation. Journal of the Taiwan Institute of Chemical Engineers, 47, 6-17.

[13] Huang, T., Yao, J., Huang, Z., Yin, X., Xie, H., & Zhang, J. (2017). Numerical simulation on ferrofluid flow in fractured porous media based on discrete-fracture model. Open Physics, 15(1), 370-378.

[14] Neuringer, J. L. (1966). Some viscous flows of a saturated ferro-fluid under the combined influence of thermal and magnetic field gradients. International Journal of Non-Linear Mechanics, 1(2), 123-137.

[15] Majeed, A., Zeeshan, A., & Ellahi, R. (2016). Unsteady ferromagnetic liquid flow and heat transfer analysis over a stretching sheet with the effect of dipole and prescribed heat flux. Journal of Molecular Liquids, 223, 528-533.

[16] Lu, D., Ramzan, M., Ahmad, S., Shafee, A., & Suleman, M. (2018). Impact of non-linear thermal radiation and entropy optimization coatings with hybrid nanoliquid flow past a curved stretched surface. Coatings, 8(12), 430.

[17] Muhammad, N., & Nadeem, S. (2017). Ferrite nanoparticles Ni-$ZnFe_2O_4$, Mn-$ZnFe_2O_4$ and Fe_2O_4 in the flow of ferromagnetic nanofluid. The European Physical Journal Plus, 132(9), 377.

[18] Hayat, T., Ahmad, S., Khan, M. I., & Alsaedi, A. (2018). Exploring magnetic dipole contribution on radiative flow of ferromagnetic Williamson fluid. Results in Physics, 8, 545-551.

[19] Crane, L. J. (1970). Flow past a stretching plate. Zeitschrift für angewandte Mathematik und Physik ZAMP, 21(4), 645-647.

[20] Gupta, P. S., & Gupta, A. S. (1977). Heat and mass transfer on a stretching sheet with suction or blowing. The Canadian Journal of Chemical Engineering, 55(6), 744-746.

[21] Chakrabarti, A., & Gupta, A. S. (1979). Hydromagnetic flow and heat transfer over a stretching sheet. Quarterly of Applied Mathematics, 37(1), 73-78.

[22] Andersson, H. I., Bech, K. H., & Dandapat, B. S. (1992). Magnetohydrodynamic flow of a power-law fluid over a stretching sheet. International Journal of Non-Linear Mechanics, 27(6), 929-936.

[23] Hayat, T., Muhammad, T., Shehzad, S. A., & Alsaedi, A. (2017). An analytical solution for magnetohydrodynamic Oldroyd-B nanofluid flow induced by a stretching sheet with heat generation/absorption. International Journal of Thermal Sciences, 111, 274-288.

[24] Ramzan, M., & Yousaf, F. (2015). Boundary layer flow of three-dimensional viscoelastic nanofluid past a bi-directional stretching sheet with Newtonian heating. AIP Advances, 5(5), 057132.

[25] Hussain, T., Shehzad, S. A., Hayat, T., Alsaedi, A., Al-Solamy, F., & Ramzan, M. (2014). Radiative hydromagnetic flow of Jeffrey nanofluid by an exponentially stretching sheet. Plos One, 9(8), e103719.

[26] Sanni, K. M., Asghar, S., Jalil, M., & Okechi, N. F. (2017). Flow of viscous fluid along a nonlinearly stretching curved surface. Results in Physics, 7, 1-4.

[27] Sharma, R., & Bisht, A. (2018). Numerical study of MHD flow and heat transfer of nanofluid along a nonlinear curved stretching surface. In AIP Conference Proceedings (Vol. 1975, No. 1, p. 030025). AIP Publishing.

[28] Afridi, M. I., Qasim, M., Wakif, A., & Hussanan, A. (2019). Second law analysis of dissipative nanofluid flow over a curved surface in the presence of Lorentz force: Utilization of the Chebyshev–Gauss–Lobatto spectral method. Nanomaterials, 9(2), 195.

[29] Sajid, M., Iqbal, S. A., Naveed, M., & Abbas, Z. (2016). Joule heating and magnetohydrodynamic effects on ferrofluid (Fe_3O_4) flow in a semi-porous curved channel. Journal of Molecular Liquids, 222, 1115-1120.

[30] Roşca, N. C., & Pop, I. (2015). Unsteady boundary layer flow over a permeable curved stretching/shrinking surface. European Journal of Mechanics-B/Fluids, 51, 61-67.

[31] Naveed, M., Abbas, Z., & Sajid, M. (2016). MHD Flow of Micropolar Fluid due to a Curved Stretching Sheet with Thermal Radiation. Journal of Applied Fluid Mechanics, 9(1).

[32] Hayat, T., Kiran, A., Imtiaz, M., & Alsaedi, A. (2016). Hydromagnetic mixed convection flow of copper and silver water nanofluids due to a curved stretching sheet. Results in Physics, 6, 904-910.

[33] Hayat, T., Qayyum, S., Imtiaz, M., & Alsaedi, A. (2018). Double stratification in flow by curved stretching sheet with thermal radiation and joule heating. Journal of Thermal Science and Engineering Applications, 10(2), 021010.

[34] Nadeem, S., Ahmed, Z., & Saleem, S. (2019). Carbon nanotubes effects in magneto nanofluid flow over a curved stretching surface with variable viscosity. Microsystem Technologies, 25(7), 2881-2888.

[35] Reddy, J. V. R., Sugunamma, V., & Sandeep, N. (2018). Dual solutions for nanofluid flow past a curved surface with nonlinear radiation, Soret and Dufour effects. In Journal of Physics: Conference Series (Vol. 1000, No. 1, p. 012152). IOP Publishing.

[36] Saba, F., Ahmed, N., Hussain, S., Khan, U., Mohyud-Din, S., & Darus, M. (2018). Thermal analysis of nanofluid flow over a curved stretching surface suspended by carbon nanotubes with internal heat generation. Applied Sciences, 8(3), 395.

[37] Soomro, F. A., Haq, R. U., Al-Mdallal, Q. M., & Zhang, Q. (2018). Heat generation/absorption and nonlinear radiation effects on stagnation point flow of nanofluid along a moving surface. Results in Physics, 8, 404-414.

[38] Ahmad, S., Farooq, M., Javed, M., & Anjum, A. (2018). Slip analysis of squeezing flow using doubly stratified fluid. Results in Physics, 9, 527-533.

[39] Rana, P., Dhanai, R., & Kumar, L. (2017). Radiative nanofluid flow and heat transfer over a non-linear permeable sheet with slip conditions and variable magnetic field: Dual solutions. Ain Shams Engineering Journal, 8(3), 341-352.

[40] Abbas, Z., Naveed, M., & Sajid, M. (2016). Hydromagnetic slip flow of nanofluid over a curved stretching surface with heat generation and thermal radiation. Journal of Molecular Liquids, 215, 756-762.

[41] O.K. Koriko, I.L. Animasaun, A.J. Omowaye & T. Oreyeni. (2019).The combined influence of nonlinear thermal radiation and thermal stratification on the dynamics of micropolar fluid along a vertical surface. Multidiscipline Modeling in Materials and Structures. 15. 133-155

[42] Muhammad ,Farooq& Alsaedi, A. (2015). Thermally stratified stagnation point flow of Casson fluid with slip conditions. International Journal of Numerical Methods for Heat & Fluid Flow. 25(4).

[43] Muhammad, N., Nadeem, S., & Haq, R. U. (2017). Heat transport phenomenon in the ferromagnetic fluid over a stretching sheet with thermal stratification. Results in Physics, 7, 854-861.

[44] Rehman, K. U., Malik, M. Y., Salahuddin, T., & Naseer, M. (2016). Dual stratified mixed convection flow of Eyring-Powell fluid over an inclined stretching cylinder with heat generation/absorption effect. AIP Advances, 6(7), 075112.

[45] Hayat, T., Nassem, A., Khan, M. I., Farooq, M., & Al-Saedi, A. (2018). Magnetohydrodynamic (MHD) flow of nanofluid with double stratification and slip conditions. Physics and Chemistry of Liquids, 56(2), 189-208.

[46] C. L. M.Navier. (1827). Surleslois Du Mouvement Des Fluides. C. R. Acad.Sci, 6, 389–440.

[47] Hone, J. (2004). Carbon nanotubes: thermal properties. Dekker Encyclopedia of Nanoscience and Nanotechnology, 603-610.

[48] Antar, Z., Noel, H., Feller, J. F., Glouannec, P., & Elleuch, K. (2012). Thermo-physical and radiative properties of conductive biopolymer composite. In Materials Science Forum (Vol. 714, pp. 115-122). Trans Tech Publications.

[49] Oztop, H. F., & Abu-Nada, E. (2008). Numerical study of natural convection in partially heated rectangular enclosures filled with nanofluids. International Journal of Heat and Fluid flow, 29(5), 1326-1336.

[50] Ebrahimnia-Bajestan, E., & Niazmand, H. (2011). Convective heat transfer of nanofluids flows through an isothermally heated curved pipe. Iranian Journal of Chemical Engineering, 8(2), 81-97.

[51] Bejan, A. (2013). Convection heat transfer. John wiley & sons.

[52] Zhang, Y., Shi, Q., Schliesser, J., Woodfield, B. F., & Nan, Z. (2014). Magnetic and thermodynamic properties of nanosized Zn ferrite with normal spinal structure synthesized using a facile method. Inorganic chemistry, 53(19), 10463-10470.

[53] Khorasanizadeh,H., Nikfar,M., and Amani,J. (2013). Entropy generation of Cu-water nanofluid mixed convection in a cavity, European Journal of Mechanics, 37(28), 143-152.